Summer 7-2018

NUMERICAL MODELING OF THE EFFECTS OF LAND USE CHANGE AND IRRIGATION ON STREAMFLOW DEPLETION OF FRENCHMAN CREEK, NEBRASKA

Moussa Guira
University of Nebraska - Lincoln, moussaguira@gmail.com

NUMERICAL MODELING OF THE EFFECTS OF LAND USE CHANGE AND IRRIGATION ON STREAMFLOW DEPLETION OF FRENCHMAN CREEK, NEBRASKA

by

Moussa Guira

A THESIS

Presented to the Faculty of

The Graduate College at the University of Nebraska

In Partial Fulfillment of Requirements

For the Degree of Master of Science

Major: Earth and Atmospheric Sciences

Under the Supervision of Professor Vitaly A. Zlotnik

Lincoln, Nebraska

August, 2018

NUMERICAL MODELING OF THE EFFECTS OF LAND USE CHANGE AND IRRIGATION ON STREAMFLOW DEPLETION OF FRENCHMAN CREEK, NEBRASKA

Moussa Guira, M.S.

University of Nebraska, 2018

Advisor: Vitaly A Zlotnik

A three-dimensional Control Volume Finite Difference-based numerical groundwater flow model was constructed to assess the effects of agricultural irrigation and land use change on streamflow depletion. The study area is Frenchman Creek basin located in southwestern corner of the State of Nebraska, USA. This area was subject to an increased proliferation of groundwater abstraction for agricultural purposes since industrial revolution with the number of irrigation wells going from 17 in 1950 to 457 in 2000; an increase of more than 2500% in 50 years. It has also been subject to land use change from native rangeland to dry and irrigated cropland. The groundwater flow model was spatially discretized using Voronoi cells in unstructured grid built with the USGS MODFLOW-6 - supported discretization by vertices (DISV) package. Temporal discretization defined 151 time steps with varying lengths and organized in 76 non-growing season time steps alternating with 75 growing season time steps and covering a period of 75 years (January 1st 1941 to December 31st 2015). The model was calibrated using PEST and against 151 streamflow measurements, 3200 groundwater level measurements, and 75 separated baseflow values. Results show that the combined application of irrigation and land use change over the study area consumed up to 98% of a portion of groundwater that would overwise discharge under the influence of ambient groundwater flow as baseflow to Frenchman Creek. A run of the model in base conditions, which consists of

maintaining land use and irrigation constant from early stage, shows that anthropogenic activities (irrigation and land use change) curtailed the amount of groundwater discharge to evapotranspiration. The study also shows the advantage of using un-structurally discretized numerical model over previously developed analytical model by Traylor and Zlotnik in accounting for aquifer heterogeneity as well as spatial and temporal changes in transmissivity.

ACKNOWLEDGEMENTS

I would like to take this opportunity to thank my wife Roukayatou Sorgho for putting up some of her priorities and supporting me during my graduate student life. I am grateful for the sacrifices she made and the emotional support that she provided to me. Special thanks go to Dr. Zlotnik for accepting to be my advisor and allowing me to further my education under his supervision. I am grateful for his commitment to support me not only academically but also beyond. Thanks for coming up with the research idea, the multiple networking opportunities, the constant push for better work, and more importantly the support and advice provided to my wife and I. I do not take it for granted. I would also like to thank my committee members, Drs. Rowe and Heeren for helpful discussions and suggestions.

I would like to recognize Philip Paitz (UNL), Zablon Adane (UNL), William Moak (UNL) and Nathan Rossman (HDR) for helpful discussions during and outside of meetings with Dr Zlotnik. I would like to thank Dr. Frank and the Department of Earth and Atmospheric Science for providing partial funding for my research. I would like to extend my thanks to the U.S. Geological Survey personnel Steve Peterson for helpful discussion and suggestions, JP Traylor for handing to me an important part of the data used in this research, and always being available for discussion and suggestions (both in Lincoln office, Nebraska) and Chris Langevin (Reston, VA) for helping me with spatial discretization as well as questions related to model development. Thank you to Salfo Bikienga (UNL) for helping with python and R programming, and along with Harrouna Malgoubri (UNL) and Lassoure Sosthene Compaore (UNL) for numerous constructive discussions on much broader subjects.

I would like to recognize the U.S. Geological Survey for streamflow data, the Nebraska Department of Natural Resources for Digital Elevation Model, well and irrigation data. Thanks

to the Upper and Middle Natural Resources Districts for irrigation data. Thanks to Aaron Young (UNL-School of Natural Resources) for providing historical groundwater data, to Jason Kennedy (Middle Republican NRD) for direct communication on irrigation and land uses practices within the Middle NRD, and guidance during my trip to the study area for field recognition. Finally, I want to thank parents and siblings for believing in me and encouraging to get this degree.

TABLE OF FIGURES

TABLE OF EQUATIONS

TABLE OF NOTATIONS

Notation	**Explanation**
∇h	Head gradient [–]
τ	Time variable used to sample numerical model outputs [T]
ς	Fraction of well screen length under saturation [–]
A^e	Surface area for Finite element e [L^2]
CC, CR, CV	Hydraulic conductances [L^2 / T]
Fm	Abbreviation for Geologic Formation
h	Hydraulic head [L]
h^e	Head within finite element e [L]
i	Stress period identifier
j	Calendar year identifier
i,j,k	Row, column and layer identifiers (indices)
K	Hydraulic conductivity [L / T]
m	Time step identifier
SS	Specific storage [L^{-1}]
Sy	Specific yield [–]
T, t	Time [T]
T	Transmissivity [L^2 / T]

TABLE OF ABREVIATIONS

Abbreviation	**Meaning**
ASCII	American Standard Code for Information Interchange
CDL	Cropland Data Layer
CVFD	Control Volume Finite Difference
DISU	Unstructured Discretization
DISV	Discretization by Vertices
DEM	Digital Elevation Model
DNR	Department of Natural Resources
FC	Frenchman Creek
FD	Finite Difference
FE	Finite Element
FORE-SCE	Forecasting Scenario
GCS	Geographic Coordinate System
GIS	Geographical Information System
GW	Groundwater
NAD	North American Datum
SFR	Streamflow Routing
SW	Surface Water
PEST	Parameter Estimation
SWC	Stinking Water Creek
USDA	United States Department of Agriculture
USGS	United States Geological Survey
UTM	Urchin Tracking Module

TABLE OF CONTENTS

Introduction

1.1 Purpose And Scope

Effective monitoring and prediction of stream depletion rates in semi-arid conditions such as the Great Plains in the US heavily relies on modeling of groundwater-surface water interactions. We are studying the joint effects of land cover change and irrigation on streamflow depletion over the Frenchman Creek Basin in Southwestern Nebraska (Figure.1-1). This area has experienced a substantial land use change in conjunction with an increased proliferation of groundwater pumping for irrigation since the start of the agricultural revolution (McGuire, 2014; Zeng, 2014; NDNR, 2015). Previous studies (McGuire, 2014; Bosh-Rubia, 2015) and field measurements (USGS, 2015) have shown significant declines of groundwater levels as well as stream discharge across the study area. Bosh-Rubia (2015) reported that the largest water level decline (greater than 24m) in Nebraska since predevelopment occurred in the Southwest corner of the Nebraska, while analytical modeling by Traylor and Zlotnik (2016) shows a large consumption of baseflow due to irrigation by the 462 wells in the area as of 2009.

Numerical modeling of groundwater is widely used as a tool to understand key factors associated with streamflow depletion (Chen and Yin, 2001; Rossman and Zlotnik, 2013). In some cases, where numerical modeling is highly challenged by paucity and unreliability of input data, water resources managers may rely on analytical modeling (Traylor, 2012) as a complementary or substitute approach. However, it is not uncommon that analytical models fail to properly simulate important hydrologic processes and characteristics, such as boundary conditions, which are well known to have significant influence on head distribution throughout the model domain and therefore on groundwater-surface water (GW-SW) interactions. For example, Chang and Yin (2001) reported that MODFLOW has advantages over an analytical

solution because it accounts for vertical flow in the vicinity of the streambed. Numerical modeling remains the leading approach for approximating predictive evolution of groundwater and surface water interactions for engineering decisions.

The objectives of this study include using some of the latest technologies to propose a numerical groundwater flow model to address the following concerns:

- Use of Control Volume Finite Difference model built on Voronoi unstructured grid using discretization by vertices (DISV) from MODFLOW-6
- To quantify the combined effects of land use change and irrigation on streamflow depletion over Frenchman Creek Basin.
- To develop a method to account for aquifer heterogeneity and changes in transmissivity
- Compare numerical model to analytical model by Traylor and Zlotnik (2016)

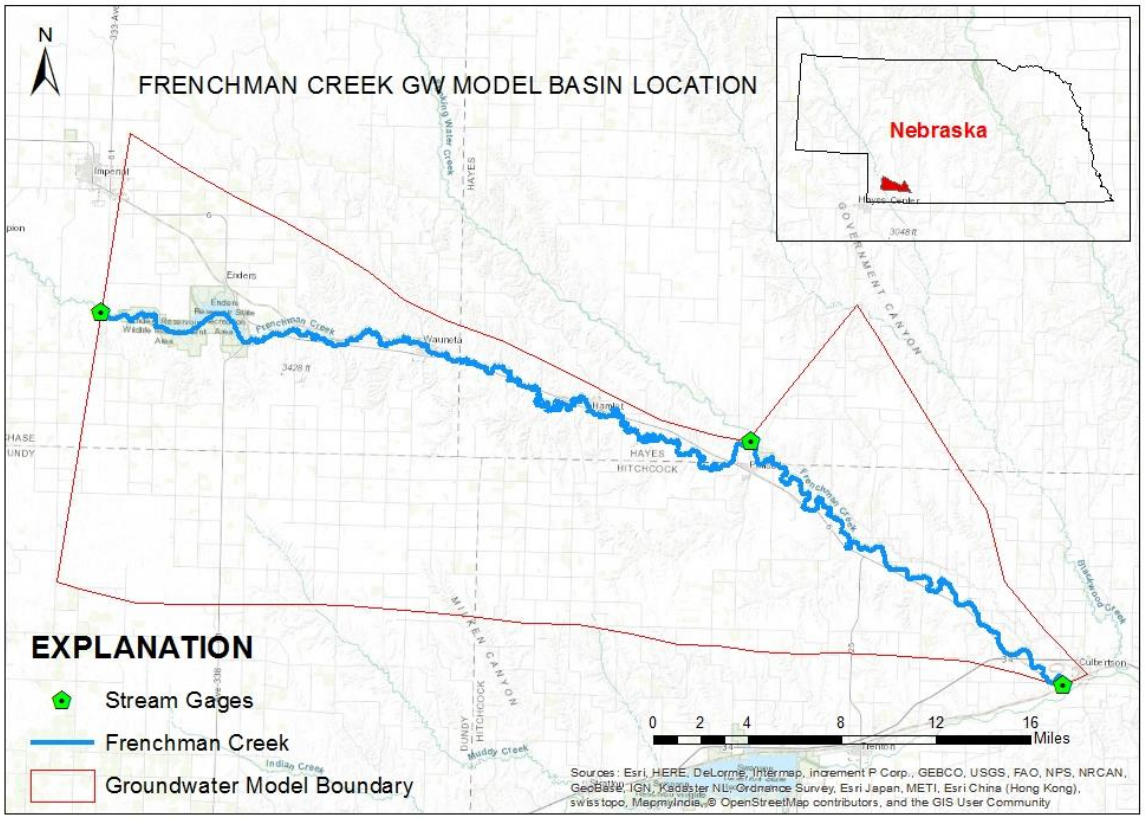

Figure 1-1: Frenchman Creek and groundwater model boundary. The inset shows the location of Frenchman Creek in Nebraska.

1.2 Study Area Description

The Frenchman Creek is a tributary to the Republican River in southwestern Nebraska (USA). The study area is the groundwater basin and includes parts of Hayes, Hitchcock, Dundy, and Chase counties. It has an area of 1308.75 km^2 (505.31 mi^2) which lies between longitudes W100.82 and W101.66 and latitudes N40.21 and N40.55. The only perennial streamflow system is Frenchman Creek which enters the domain from the west, 10 km southeast of Champion, NE and flows through the area in southeastward direction and exits at Culbertson, NE. The basin lies entirely within the High Plains section of the Great Plains Physiographic province (Fenneman,

1931). Traylor and Zlotnik (2016) reported that there was approximately 191 km^2 of terraced lands within the basin, with most of them having been installed between 1950 and 1970. Area with agricultural land use in the modeled part of the basin represents a significant part of the model domain with 2009 estimates of more than 90%; the other 10% being covered by open water, roads, riparian areas and wetlands (Traylor, 2012). There was a steady decline in dry cropland between 1960 and 1980 as dry croplands were being converted into irrigated land. A Digital Elevation Model (DEM) of the land surface in the area shows that elevation ranges between 1056 m in the western side of the domain (near Enders Reservoir) and 785 m at the eastern end (Culbertson). Figure 1-2 shows a Digital Elevation Model (DEM) of the land surface.

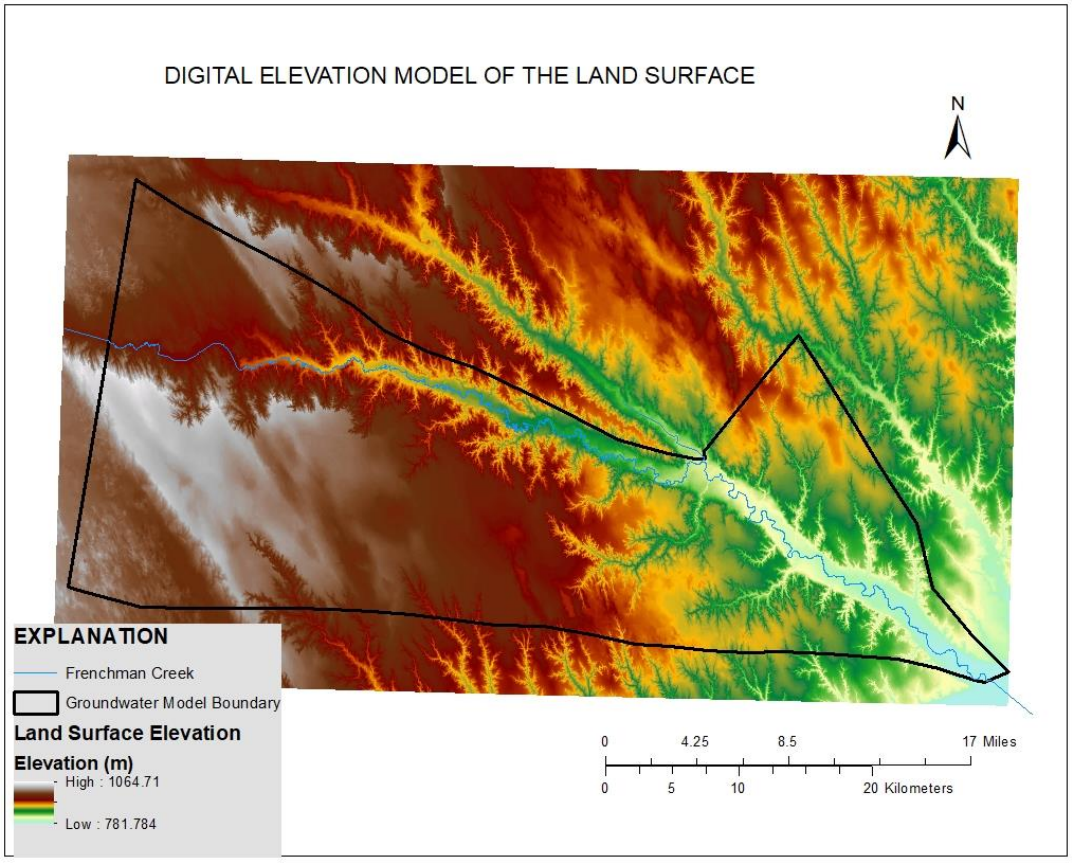

Figure 0-2: Digital Elevation Model (DEM) showing the land surface altitude with respect to North American Datum (NAD83)

1.3 Previous Studies

The first detailed hydrologic study involving Frenchman Creek goes back to 1907. In a study of the geology and water resources of the Republican River Valley based on seasonal observations and 1904 summer field work, Condra (1907) referred to Frenchman Creek as Frenchman River. This designation was essentially due to the impressions of then-existing significant flows, unlike in recent observations. Caldwell and Jenkins (1963) used analytical methods to provide the first estimates of stream depletion due to groundwater abstraction by wells. They also predicted future water level declines due to irrigation in a larger area including the Frenchman Creek (FC) basin. A numerical model of the Upper Republican Natural Resources District by Lappala (1978) predicted future groundwater levels and streamflow declines whether irrigation development continued at then current rate or ended in 1976. In 1995, Peckenpaugh et al. (1995) updated Lappala's model using MODFLOW, with the focus on the effects of irrigation well pumping on groundwater levels. Both Lappala and Peckenpaugh models cover a substantial part of the FC basin but leave out the eastern half. Findings from studies by Szilagyi (1999, 2001), and Burt et al. (2002) support the conclusion that groundwater level decline is due to anthropogenic activities and not a result of climate change. An analysis of water level change by McGuire (2014) shows that some of the greatest declines in Nebraska since predevelopment occurred in this study area. Zeng and Cai (2014) used a modified Soil and Water Assessment Tool (SWAT) to link baseflow to changes in storage over FC surface water basin area and evaluated streamflow decline from wells. The SWAT model however is based on the surface water basin which does not fully account for the groundwater basin. A delineated groundwater basin based on water table equipotential lines shows that an area subject to

significant groundwater withdrawals and hydraulically connected to the stream would have been omitted by the SWAT model.

Finally, analytical modeling by Traylor and Zlotnik (2016) over our study area showed that pumping from 462 irrigation wells consumed a large portion of baseflow. Groundwater inflow to the basin was described in the analytical model as a constant. This assessment assumed a constant cross section of the aquifer area and a constant hydraulic gradient, hence constant saturated thickness and transmissivity. Their analytical model does not account for spatial variability of aquifer parameters and finite aquifer boundaries. Therefore, while their model is able to replicate the baseflow consumption by wells, some bias in aquifer parameter estimates is possible.

Hydrogeology

1.4 Major Hydrogeologic Units

An aquifer is a subsurface layer that easily stores and transmits water (Hendricks, 2010). Freeze and Cherry (1979) reported that in the water well industry, an aquifer is a subsurface layer that is permeable enough to yield economic quantities of water to wells. This definition makes it clear that the ability to release water is a requirement for a subsurface body to be considered an aquifer; otherwise the layer might fall into the aquitard or aquiclude categories. An aquitard is a geologic subsurface layer that is semi-permeable (Hendricks, 2010) and can become a confining unit when it overlays an aquifer, whereas an aquiclude is permeable enough to transmit water in a regional scale but cannot yield enough water to wells to be economically profitable (Freeze and Cherry, 1979).

The major hydrologic unit on which this study is based is the Ogallala aquifer, an important component of the High Plains Aquifer. The Ogallala aquifer is essentially composed of the Ogallala formation, which was deposited during the Miocene Epoch (23.03-5.33 million years ago) (Burchett, 1986; USGS, 2018). The Ogallala Fm is broadly characterized by lenses and tabular zones of carbonate-cemented silt and sand. In a few localities, fine to coarse sand and fine gravel are cemented by opal or chalcedony. Some volcanic ash beds are also found in a few deposits (Burchett, 1986; Diffendal, 1991; USGS, 2018). Sedimentation and lithology vary vertically and laterally within short distances which is why more localized descriptions based on counties are available. The Ogallala Fm is consistent across the four counties (Chase, Dundy, Hayes, and Hitchcock) that this study area encompasses. It is characterized by silt, sand, sandstone and conglomerate, mostly interfingered with fine- to coarse-grained, poorly-sorted,

arkosic, fluvial deposits. The color of those deposits ranges from light gray to grayish green. Calcareous silt and poorly consolidated conglomerate as well as sandstone and siltstone are found in local beds (USGS, 2018). The Ogallala Fm has a relatively low permeability but with its considerable thickness and extent, it remains the unit that stores most of the groundwater of the High Plains Aquifer (Peterson et al, 2016).

The other geologic unit with water storing capacity is the alluvial aquifer which was mapped along the valleys of Frenchman and Stinking Water Creeks by Caldwell et al. (1963). The alluvial aquifer in the study area started depositing in early Pleistocene (2.58 million years ago) and consists of clay, silt, and channel deposits of sand and gravel (Caldwell et al., 1963; USGS, 2018) which are the most permeable material in the basin.

It is important to note that underlying the Ogallala Fm are units with poor water storage and conductivity which make them less suitable for well development. Directly underlying the Ogallala Fm is the White River Group composed of Brule and Chadron Formations. Unconformably underlying the White River Group is the Pierre Shale which is the poorest water bearing material in the basin (Caldwell et al., 1963). For the purpose of this study, only the Ogallala and the alluvial aquifers are considered.

1.5 Aquifer Base Altitude And Saturated Thickness

In this study, we define the aquifer as the water holding geologic body within the geographic extent of the study area. This includes both the Ogallala and alluvial aquifers due to their high-water-storing capacity. The underlying materials, the White River Group and the Pierre Shale, which have significantly lower storage capacities are not taken to account. Therefore, the base of the aquifer here refers to the bottom of the Ogallala aquifer or the base of alluvial aquifer where it is in contact with the lower water storing capacity body. Base altitude

data were taken from the data released in the Northern High Plains Aquifer groundwater availability study by Peterson et al. (2016). Initial saturated thickness is computed by subtracting base altitude from predevelopment GW levels by McGuire (2014). Saturated thickness changes dramatically across the model domain with the highest values (as high as 254 meters) along the western boundary. Saturated thickness is thinning eastward with some of the lowest values around Culbertson where FC exits the model domain (Figure 2-1). Base altitude corrections were made where initial calculated saturated thicknesses were negative. Using well screen depth information, we changed base altitude to satisfy a minimum saturated thickness of 5 meters. Thus, all model cells with saturated thickness less than five meters were brought up to five meter.

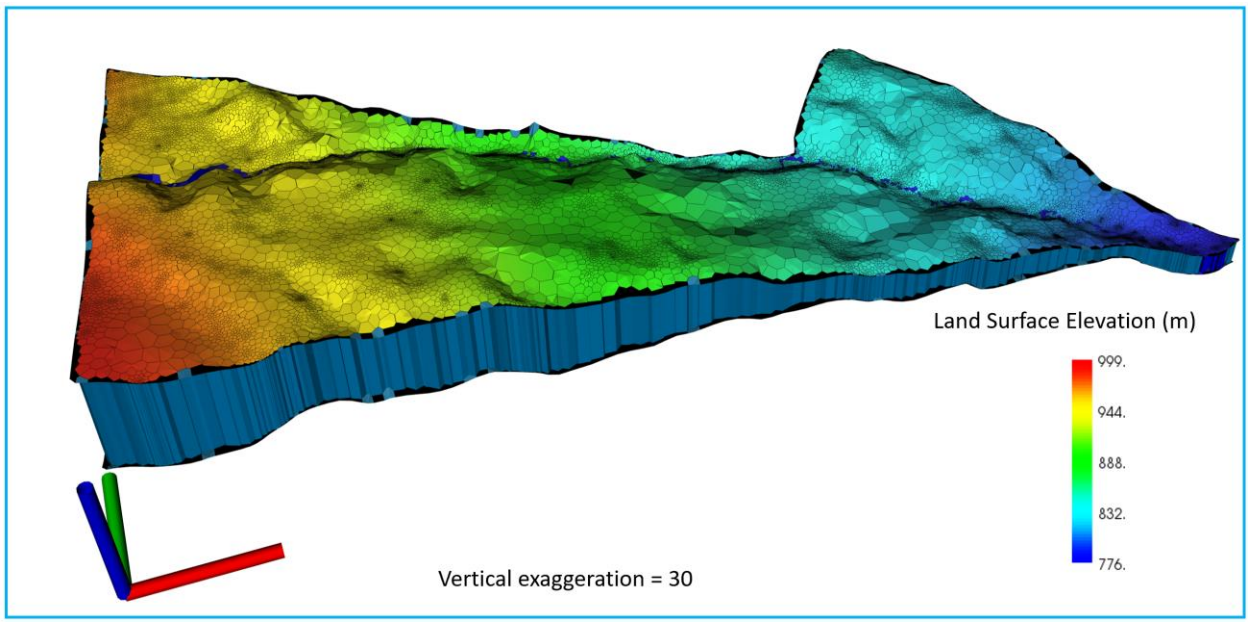

Figure 2-1: 3-D representation of the model sowing aquifer thickness. Aquifer is thinning eastward

Numerical Groundwater-Flow Modeling

1.6 Requirements For The Model

A numerical groundwater flow model is a data-driven simplified representation of complex hydrological conditions in the subsurface (Anderson et al., 2015). Mathematical groundwater flow models simulate spatial and temporal distribution of hydraulic head (Anderson et al., 2015). Process-based mathematical groundwater flow models use governing equations which describe or approximate physical processes that occur within a predefined model domain. Numerical groundwater models use input data that specify initial and boundary conditions. Initial conditions are head values within the model domain at the beginning of the simulation whereas boundary conditions specify heads and/or fluxes across the boundaries. Boundaries are the interfaces between model and exterior through which exchanges may or may not be allowed.

1.7 Selecting Software

1.1.1. General Principles

Because of their simplistic nature compared to real world situations, every model including groundwater flow model has its limitations with respect to being able to simulate processes. It is a consensus that software packages used in groundwater modeling have improved over time with added capabilities of simulating more complex processes. It is, however, important to note that all groundwater flow models simulate flow based on Darcy's Law (Equation 3-1). In a three-dimensional setting, the movement of groundwater of constant density through subsurface porous media is characterized by Darcy's Law as

$$q = -K\nabla h = -\begin{pmatrix} K_{xx} & 0 & 0 \\ 0 & K_{yy} & 0 \\ 0 & 0 & K_{zz} \end{pmatrix} \nabla h, \tag{3-1}$$

In (3-1), q (a vector) is specific discharge [L.T^{-1}], K is the hydraulic conductivity tensor (L/T) composed of K_{xx}, K_{yy}, and K_{zz}, the values of the hydraulic conductivity along the x, y, and z axes. h is the potentiometric head (L) and ∇h is the gradient of head (a vector).

Applying the water balance to a small control volume, Equation 3-1 leads to a partial differential equation (3-2), responsible for the distribution of hydraulic head (McDonald and Harbaugh, 1988)

$$\frac{\partial}{\partial x}\left(K_{xx}\frac{\partial h}{\partial x}\right)+\frac{\partial}{\partial y}\left(K_{yy}\frac{\partial h}{\partial y}\right)+\frac{\partial}{\partial}\left(K_{zz}\frac{\partial}{\partial z}\right)+Q_s=SS\frac{\partial h}{\partial t}, \qquad (3\text{-}2)$$

where Q_s is a parameter representing the volumetric flux per unit volume of sources and sinks of water with respect to the groundwater flow system [T^{-1}]. Thus, a sink such as transpiration would be represented by a negative contribution to Q_s whereas a source such as deep percolation would be represented by a positive contribution to Q_s. SS is the specific storage [L^{-1}], and t is the time [T].

Typically, numerical groundwater flow models are based on either finite-difference (FD) or finite-element (FE) methods. Each method has been used to develop very well-known software packages, capable of simulating steady-state and transient groundwater flow conditions.

Using the FD method in rectangular discretization, and adding initial and boundary conditions to Equation 3-2, we obtain the transient three-dimensional groundwater flow equation in a heterogeneous and anisotropic environment. This assumes that the principal axes of hydraulic conductivity are aligned with the coordinate directions. The discretization calls for each cell to be represented by a single node for which head is calculated (McDonald and Harbaugh, 1988, 2003). The transient finite difference equation for a grid cell is

$$CR_{i,j-\frac{1}{2},k}(h^m_{i,j-1,k} - h^m_{i,j+1,k}) + CR_{i,j+\frac{1}{2},k}(h^m_{i,j+1,k} - h^m_{i,j,k}) + CC_{i,j-\frac{1}{2},k}(h^m_{i,j-1,k} - h^m_{i,j+1,k}) \quad (3\text{-}3)$$

$$+CC_{i,j+\frac{1}{2},k}(h^m_{i,j+1,k} - h^m_{i,j,k}) + CV_{i,j-\frac{1}{2},k}(h^m_{i,j-1,k} - h^m_{i,j+1,k}) + CV_{i,j+\frac{1}{2},k}(h^m_{i,j+1,k} - h^m_{i,j,k})$$

$$+P_{i,j,k}h^m_{i,j,k} + Q_{i,j,k} = SS_{i,j,k}(DR_j \cdot DC_i \cdot DV_{i,j,k})\frac{h^m_{i,j,k} - h^m_{i,j,k}}{t^m - t^{m-1}}$$

where

$h^m_{i,j,k}$ (L) is head at cell found at the intersection of row i, column j, and layer k at time step m.

CR, CC, and CV are hydraulic conductances between cell (i,j,k) and the contiguous cell respectively along rows, columns, and layers; the dimension of a conductance is [L^2T^{-1}]

$P_{i,j,k}$ [L^2T^{-1}] is the sum of coefficients of heads from sources and sinks

$Q_{i,j,k}$ [L^3/T] is the sum of constants from sources and sinks with negative values depicting flow out of the groundwater and positive values depicting flow in.

$SS_{i,j,k}$ [L^{-1}] is the specific storage

DC_i [L] is cell width of row i in all columns

DR_j [L] cell width of column j in all rows

$DV_{i,j,k}$ [L] is the vertical thickness of cell (i,j,k)

t^m [T] is the time at time step m

The most popular FD-based computer program used in groundwater modeling is the USGS' MODFLOW which was released in multiple versions over the past decades. MODFLOW is well known to the modeling community around the world and is very well documented. Software like Visual MODFLOW, Argus ONE, GMS, Groundwater Vistas, and Leapfrog Hydro are commercial programs that run on some versions of MODFLOW.

In the FE method, the three-dimensional spatial discretization is a mesh of volumetric and polygonal elements defined by nodes and for which hydraulic head is represented as a continuous solution within the element (Anderson et al., 2015). Although a large variety of shapes and node locations can be used, the most commonly used finite element meshes have triangular or quadrilateral base (Anderson, 1982; Anderson et al., 2015; Wang and Anderson, 1995). Using a triangular element (Figure 3-1), a trial solution for head within the element is defined using interpolation functions known as basis functions of heads at the nodes forming the element. The general form of the linear interpolation function in a two-dimensional setting is

$$h^e(x, y) = a_0 + a_1 x + a_2 y \tag{3-4}$$

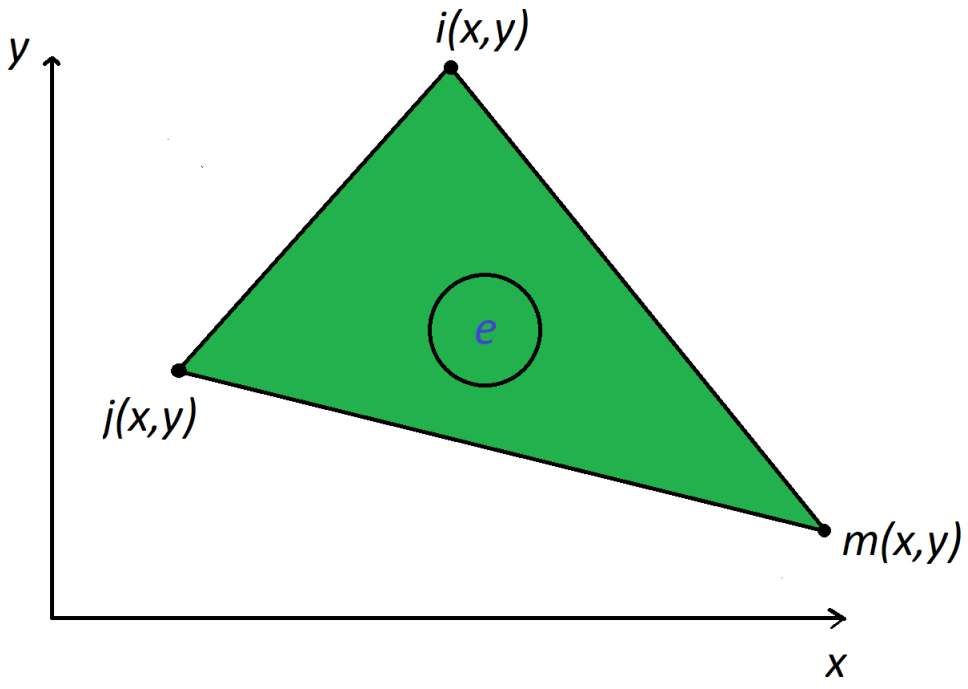

Figure 3-1: Two-dimensional triangular representative finite element. Nodes i,j, and m labelled in counterclockwise order with spatial coordinates (x,y)

where $h^e(x, y)$ is the head within the element *e* and a_0, a_1, and a_2 are coefficients determined by solving a system of head equations at the nodes *i, m,* and *j* , thus numbered counterclockwise in element *e.*

$$h_i = a_0 + a_1 x_i + a_2 y_i$$

$$h_j = a_0 + a_1 x_j + a_2 y_j \tag{3-5}$$

$$h_m = a_0 + a_1 x_m + a_2 y_m$$

Substituting a_0, a_1, and a_2 for their respective expressions from Equation 3-5, Equation 3-4 can be rewritten as:

$$h^e(x, y) = N_i^e(x, y)h_i + N_j^e(x, y)h_j + N_m^e(x, y)h_m \tag{3-6}$$

where

$$N_i^e(x, y) = \frac{1}{2A^e}\left[\left(x_j y_m - x_m y_j\right) + \left(y_j - y_m\right)x + \left(x_m - x_j\right)y\right]$$

$$N_j^e(x, y) = \frac{1}{2A^e}\left[\left(x_m y_i - x_i y_m\right) + \left(y_m - y_i\right)x + \left(x_i - x_m\right)y\right] \tag{3-7}$$

$$N_m^e(x, y) = \frac{1}{2A^e}\left[\left(x_i y_j - x_j y_i\right) + \left(y_i - y_j\right)x + \left(x_j - x_i\right)y\right]$$

and

$$A^e = \frac{1}{2}\left[\left(x_i y_j - x_j y_i\right) + \left(x_m y_i - x_i y_m\right) + \left(x_j y_m - x_m y_j\right)\right] \tag{3-8}$$

$N_i^e(x, y)$, $N_j^e(x, y)$, and $N_m^e(x, y)$ are the basis functions and they define head within the triangular element *e* of area A^e. Also N^e varies linearly from 1 at the corner where it is defined to 0 at the other corners, taking the value of 1/3 at the centroid of the triangular element.

The FE method provides an advantage over the standard FD method due to grid flexibility. Because a large variety of element shapes and spatial location of nodes, users can define elements along model boundaries in a way that greatly minimizes errors and avoids having cells outside of the active model domain. Computer programs that use an FE method for solving the groundwater flow equation include FEFLOW (Diersch, 2005), SVFLUX (Fredlund, 2010), FEHM (Zyvoloski, 2007), and others. However, due to the high level of complexity involved with nodes' x,y,z coordinates data along with computer memory requirement during code execution (Anderson et al., 2015), there has not been as much use of the FE method as the FD method in groundwater model development.

The Control Volume Finite Difference (CVFD) method is based on applying FD approach to volumetric elements. It is a type of finite volume method (Anderson et al.,2015) that supports grid flexibility but has the advantage of solving for a single head value per cell as opposed to the continuous solution used in an FE method. When Equation 3-2 is integrated over a small control volume V, it leads to

$$\int_V \left(K\nabla h\right) dV = \frac{\partial}{\partial t}\int_V (S_s h) dV + C \tag{3-9}$$

Converting the volume integral to a surface integral gives

$$\int_s \left(K\nabla h\right) n \cdot dS = S_s V \frac{\partial h}{\partial t} + W \cdot V \tag{3-10}$$

where *n* is an outward pointing unit normal vector on the volume surface and S is the surface of the control volume (Panday et al., 2013).

The CVFD method has been lately used by the USGS in the development of recent MODFLOW versions. The MODFLOW family of groundwater models has evolved throughout the last four decades; the next section of this document presents different versions of

MODFLOW, their capabilities, and ultimately helps in the understanding of our choice of software used in this study.

1.1.2. MODFLOW Family

1.1.2.1. MODFLOW-84, MODFLOW-88, and MODFLOW-96

The USGS, as part of its overall mission to provide unbiased hydrologic data and scientific analyses to support management decisions, developed a wide variety of computer models during the past four decades (McDonald and Harbaugh, 2003; Barlow and Harbaugh,2006). The models were developed and modified by hydrologists to suit their modeling needs but were limited by not being portable across computer brands (McDonald and Harbaugh, 2003). In order to address those limitations and increase efficiency, the USGS took steps to reconcile the many capabilities into one model. An initial attempt to revise an existing model by a committee in 1981 failed and led Michael McDonald and Arlen Harbaugh to develop an entirely new program with the capability of the existing ones. Initially known as the USGS Modular Three-Dimensional Finite Difference Ground Water Flow Model, the model became known as MODFLOW several years later (McDonald and Harbaugh, 2003). The first MODFLOW core version, initially developed and released as a groundwater flow simulation code was MODFLOW-84. This version, along with the second and third versions (MODFLOW-88 and MODFLOW-96) were based on the primary conceptualization of groundwater flow simulation (Harbaugh and McDonald, 1996). Updates from one core version to the next were chiefly based on release of new Fortran versions, addition of new packages, and/or fixing a bug which prevented all or parts of the model to successfully simulate processes. For instance, MODFLOW-84 was released in Fortran 66 whereas MODFLOW-88 was released of Fortran 77 (McDonald and Harbaugh, 1988).

1.1.2.2. MODFLOW-2000

This version of MODFLOW came as an update to MODFLOW-96. It has an enhanced modular structure which allows for including additional capabilities such as solute transport and parameter estimation (Harbaugh et al., 2000). The four processes included in this version are groundwater flow, sensitivity, observation, and parameter estimation. Many improvements were brought to the first MODFLOW-2000 release and as of March 2010, many (23) "bugs" were fixed, and packages were renewed or added making the final version a model that supports a total of 33 packages. MODFLOW-2000 simulates steady and non-steady groundwater flow in confined and unconfined aquifers.

1.1.2.3. MODFLOW-2005

MODFLOW-2005 (Harbaugh, 2005) was the fourth core version of MODFLOW to be released. In this version, parameter estimation—which was implemented in MODFLOW-2000—was removed along with the sensitivity analysis and the uncertainty evaluation capabilities (Schmid et al., 2006). The groundwater flow simulation is done using a block centered finite difference approach with confined or unconfined layers (Harbaugh, 2005). Flow associated with wells, areal recharge, evapotranspiration (ET), drains, and rivers, also referred to as external stresses are supported in this version. Subsequent versions developed under this core include:

- MODFLOW-CFP (Reiman and Hill, 2009) with the capability of simulation of turbulent or laminar groundwater flow condition as conduit flow processes.
- MODFLOW-LGR (Mehl and Hill, 2006) with local grid refinement capability which is useful for improving simulation in areas of interest within a relatively coarsely discretized model.

- MODFLOW-NWT (Niswonger et al., 2011) which introduced the Newton formulation to MODFLOW-2005, used to address problems with drying and rewetting related to non-linearity of the unconfined groundwater flow equation.
- MODFLOW-USG (Panday et al., 2013) which introduced the CVFD method along with unstructured grid spatial discretization to the MODFLOW family.

1.1.2.4. MODFLOW-OWHM

MODFLOW One Water Hydrologic Model (MODFLOW-OWHM) (Hansen et al., 2014) is a MODFLOW based and fully integrated model that simulates the conjunctive use water. Conjunctive use refers to the combined use of surface water and groundwater within the model domain. MODFLOW-OWHM is based on farm process package previously developed for MODFLOW-2005. The model is the result of a merger of five versions of MODFLOW (NWT, FMP, LGR, SWR, and SWI) and provides the ability to simulate demand-driven and supply-limited hydrologic processes (Hanson et al., 2014).

1.1.2.5. MODFLOW-6

The sixth core version of MODFLOW known as MODFLOW-6 (Langevin et al., 2017) was released by the USGS in September of 2017. This version came as a way of bringing all capabilities in previous versions to a single model. Many of the previous versions of MODFLOW were equipped with various simulation capabilities without necessarily being compatible across versions. MODFLOW-6 was rewritten as an object-oriented model that addresses compatibility issues and includes the ability to simulate processes with models and non-structured spatial discretization. It consolidates popular capabilities from MODFLOW versions 2005, LGR, NWT, USG, and more. It has a modernized code and input structure and still provides an improved solution technique. Furthermore, MODFLOW-6 supports multi-model

simulations. In this case, simulation timing information is controlled at the simulation level where time steps are determined and applied to all models. Exchange between models are defined at simulation level as well and the numerical solution for all models is solved at the matrix level.

MODFLOW-6 is the first of the MODFLOW family to support the discretization by vertices, another way of defining model cells that had not been implemented in MODFLOW before. It provides the flexibility of defining both structured and unstructured grids. The latter is particularly useful in accommodating complex model shapes, just like the in MODFLOW-USG and the two-dimensional FE grid. However, the level of complexity is significantly reduced, and the control volume formulation permits solving for a single head value per cell. Moreover, MODFLOW-6 supports the advanced streamflow routing package which was unstable in earlier versions with discontinuous water table across model top layer. This along with the other advantages mentioned above led us to choose MODFLOW-6 for this study.

Application Of MODFLOW-6 To Frenchman Creek

1.8 Conceptual Model

A conceptual model is a narrative description of the main physical components of the numerical model. Haitjema (1995) defines a conceptual groundwater flow model to be a simplification of a real-world groundwater problem which captures the essential features and can be mathematically represented. A conceptual model of groundwater flow was used to design the groundwater model. An early version of the model was created and updated to better represent the groundwater system as input hydrologic data were being added.

Groundwater in the study area generally flows in a southeast direction. It is however important to note some local differences in flow direction. Thus, flow near the southern boundary is nearly eastward whereas flows in the vicinity of the northern and northeastern boundaries are south-southeastward.

Water budget components of the groundwater system in the basin are positive for inflows, and negative for outflows in such a way that the sum (ΔS)is zero when the system is in steady state

$$\sum_i (Inflows)_i - (Outflows)_i = \Delta S \qquad (4.1)$$

where i represents a stress period. In this modeling effort, the number of days in i changes from one stress period to the next (see temporal discretization in section 4.2.2 and appendix D).

In this case, inflows to the model are groundwater flow across the western boundary ($GW_{in-West}$), flow across the northeastern boundary ($GW_{in-northeast}$), groundwater recharge (Rch_{in}) also knowns as deep drainage or deep percolation from both rainwater and irrigation inefficiencies, stream leakage from the streamflow routing (SFR) network (SFR_{in}), and water released from aquifer storage (STO_{in}). Outflows from the model are chiefly composed of

groundwater abstraction by irrigation wells (WEL_{out}), evapotranspiration (ET_{out}), water going into storage (STO_{out}), and baseflow to the SFR network (SFR_{out}).

Substituting *Inflows* and *Outflows* in Equation (4.1) with their components and assuming steady state, we obtain

$$GW_{in-West(i)} + GW_{in-northeast(i)} + SFR_{in(i)} + Rch_{in(i)} + STO_{in(i)} - WEL_{out(i)} - SFR_{out(i)} - ET_{out(i)} - STO_{out(i)} = 0 \quad (4.2)$$

Changes in storage are outputs from the model and one part of the modeling objectives is to calculate the aquifer storage using storage coefficient and specific yield parameters. These aquifer intrinsic parameters are determined through calibration.

In Equation 4.2, we can lump the storage terms $STO_{in(i)}$ and $STO_{out(i)}$ into a single term ΔS_i representing change in storage for stress period i. Another term can be defined from combining $SFR_{in(i)}$ and SFR_{out} into $BF_{(i)}$ representing baseflow to the river such that:

$$BF_{(i)} = SFR_{out(i)} - SFR_{in(i)} \quad (4.3)$$

The baseflow term is purposefully defined this way so that positive terms represent a gain for the stream and consequently, negative terms represent a loss. This allows us to rewrite Equation 4.2 as

$$GW_{in-west(i)} + GW_{in-northeast(i)} + Rch_{in(i)} - \Delta S_{(i)} - WEL_{out(i)} - BF_{(i)} - ET_{out(i)} = 0 \quad (4.4)$$

1.1.3. Model Domain

The spatial extent of the groundwater model domain in this study is identical to that described in the analytical model by Traylor and Zlotnik (2016). The western edge of the domain is 31.06 km long. A cross section of the aquifer through that line (AA′ on Figure 4-1) defines a

vertical surface of groundwater inflow to the domain. A similar configuration is defined along cross section BB′ (Figure 4-1) which is 11.22 Km long. A shorter length along with lower aquifer thickness in that region suggests a relatively smaller surface of groundwater inflow compared to the one at the western boundary. The stream gage at B′ is on the Stinking Water Creek tributary and therefore the watershed upstream was not included in this model.

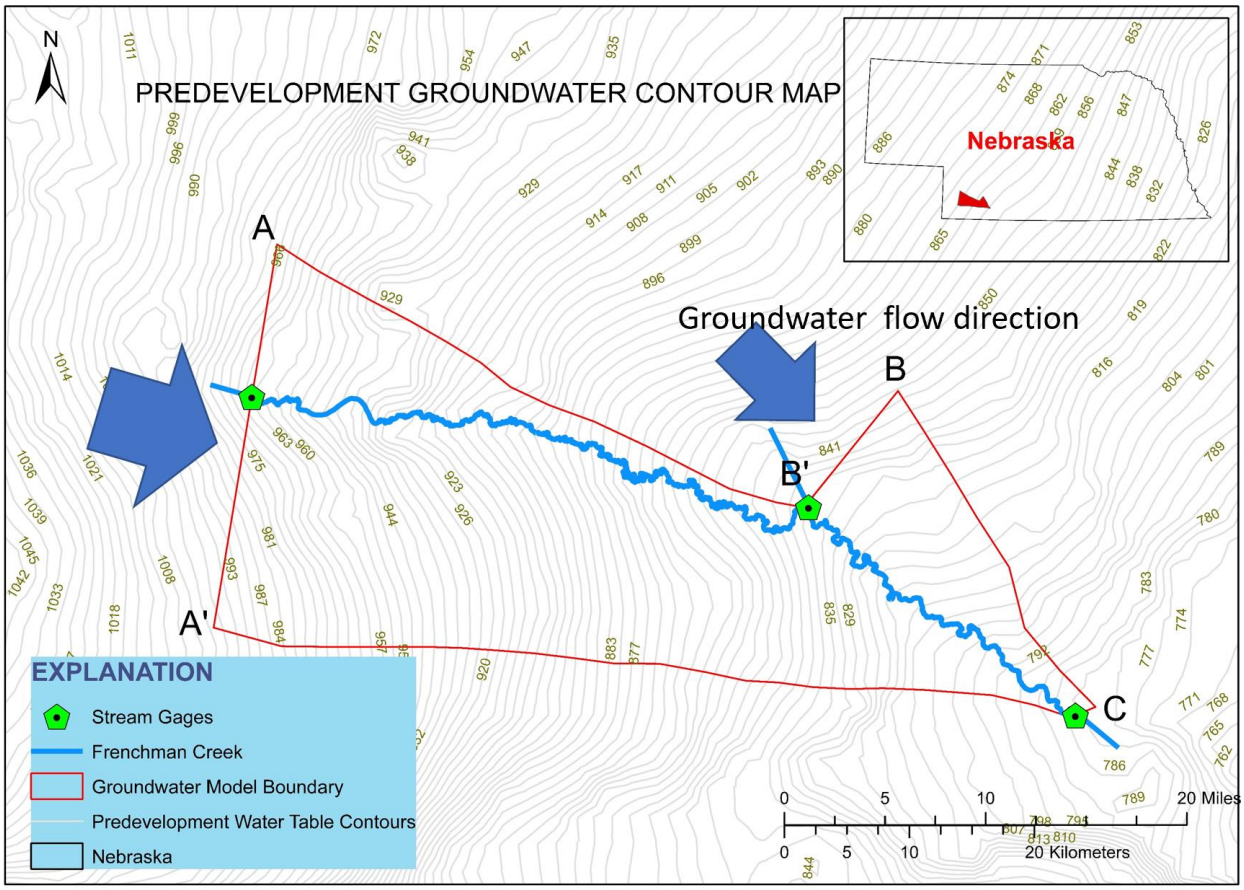

Figure 4-1: Predevelopment water table contour lines. Labelled contour lines show the highest elevation on the western end with values ranging between 965 and 1000 meters. The eastern end has the lowest elevation with values around 780 meters. The groundwater model boundary crosses the contours lines at a 90 degrees angle along segments AB', BC, and A'C, thus justifying the no-flow condition along those borders.

1.1.4. Boundary Conditions

1.1.4.1. Prescribed Head Boundary

A dynamic prescribed or specified head boundary is defined along AA′ and BB′. The water table map (Figure 4-1) shows that regional flow in the area is west-east as determined from the gradient of the contour lines. As a result, groundwater flow is primarily from these segments to the domain. Occasionally, groundwater recharge near the specified head boundary can be high enough in a relatively short time that it creates a mound where head is higher. In that case, water flows from the mound to the prescribed head boundary. These instances are short-lived and affect only a small portion of the model. It does not change the overall groundwater flow which is governed by groundwater head gradient as described by Darcy's Law, used to calculate the volumetric rate of discharge across an area

$$Q = -K \bullet A \frac{dh}{dl} \tag{4.5}$$

where Q [$L^3.T^{-1}$] is the volume of water per unit time, K [$L.T^{-1}$] is the saturated hydraulic conductivity, A [L^2] is the area perpendicular to water flow, and $\frac{dh}{dl}$ [$-$] is the hydraulic gradient. The hydraulic gradient oftentimes noted as i is the change in head dh divided by the distance travelled dl. Water is always flowing from high to low head values; as a result, dh, which is $h_{final} - h_{initial}$, is always negative hence the negative sign in the equation to ensure that discharge is positive.

1.1.4.2. Stream

In this study, Frenchman Creek is the only perennial streamflow system. In this modeling effort, the stream is represented by a network of reaches characterized by a set of parameters including stream width and riverbed conductivity. A reach is a portion of the stream network that

lies within one model cell These parameters contribute in defining the extent to which groundwater can interact with the stream. The interaction between groundwater and surface water is defined by the hydraulic gradient shown in Equation 4.5. However, in this case, there is a vertical flow component that needs to be accounted for. When a given stream reach has a stage that is lower than the piezometric surface of the groundwater model cell that contains the reach, then water flows from the aquifer to the stream as baseflow (Figure. 4-2-A). Conversely, if head in the aquifer is lower than the stage in the stream reach, then surface water is lost to the aquifer as stream leakage (Figure. 4-2-B). Besides the hydraulic gradient, the rate of this exchange is also tied to the streambed conductance which is a function of conductivity and thickness, stream length and width, and a dimensionless cubic saturation function (Equation 4-6). Conceptually, the flow between a stream reach and the underlying groundwater flow cell is computed with the assumption of uniform flow conditions using Darcy's Law:

$$Q_{SFR(reach)} = S^{*}_{SFR(reach)} \frac{K_{reach} L_{reach} W_{reach}}{b_{reach}} (H_{SFR(reach)} - h_{reach}) \tag{4-6}$$

where:

$Q_{SFR(reach)}$ is the discharge across streambed $[L^3 / T]$,

$S^{*}_{SFR(reach)}$ is cubic saturation function $[-]$,

K_{reach} is the streambed hydraulic conductivity of the reach $[L / T]$,

L_{reach} is the length of the reach $[L]$,

W_{reach} is the width of the reach $[L]$,

$H_{SFR(reach)}$ is the simulated stage of the reach $[L]$, and

h_{reach} is the hydraulic head at the cell directly underling the reach $[L]$

In this modeling effort, we use MODFLOW-6 compatible Stream Flow Routing (SFR6) package (Langevin et al., 2017) to simulate FC and the canals (Culbertson and Riverside). The SFR network comprises 1673 (*nreaches*) reaches including 1553 for FC and 128 for canals.. The "Packagedata" block of the SFR package contains information for the physical and hydrologic properties for each reach:

- *nreaches*: single identifying number for the reach
- *layer*: layer number containing the reach
- *cellID*: the number associated with the cell in the 2-dimensional discretization
- *length*: the length of the stream or canal in the reach
- *rwid*: reach width
- *rtop*: top elevation of the reach streambed
- *rbth*: streambed thickness in the reach
- *rhk*: streambed hydraulic conductivity
- *man*: Manning's roughness coefficient
- *ncon*: number of reaches connected to the current reach
- *ustrf*: upstream routing fraction
- *ndv*: number of canal diversions associated with the reach
- *boundname*: optional name used to classify the reach as being either stream or canal

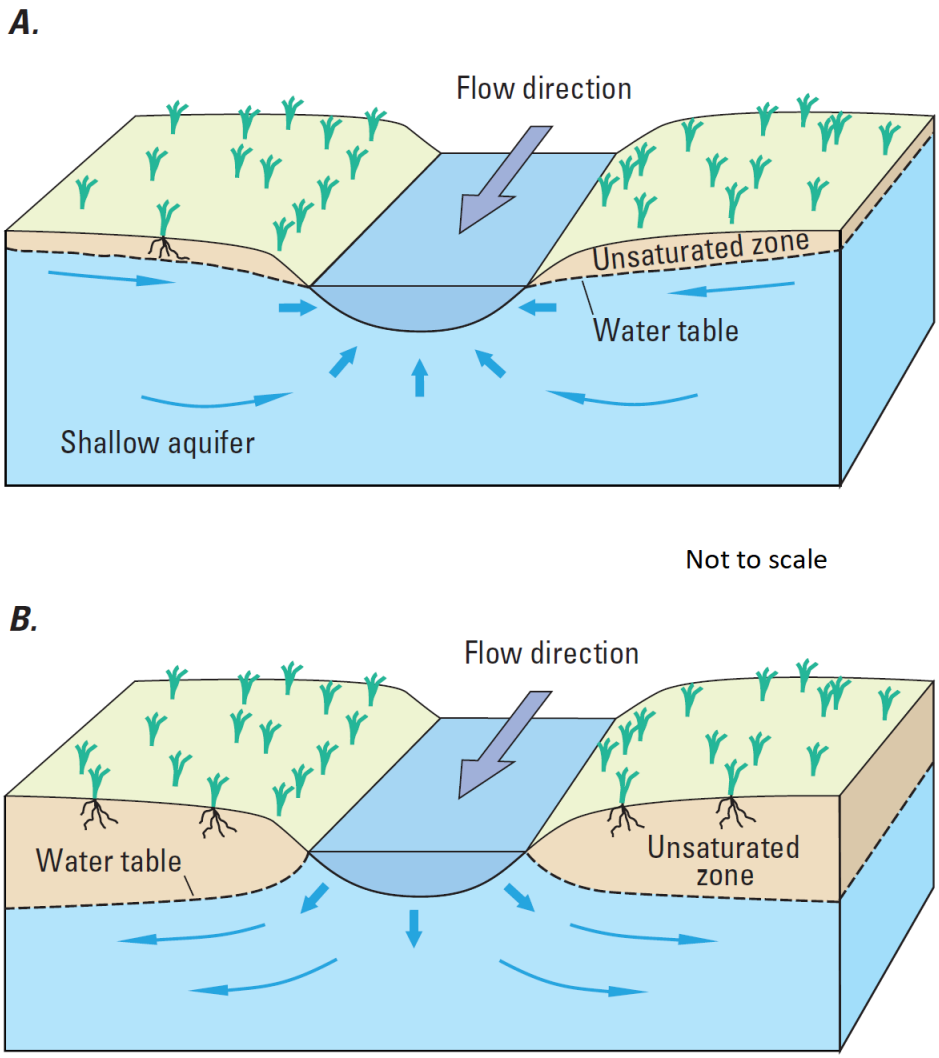

Figure 4-2: Stream-aquifer interactions. A. Gaining stream, receiving baseflow from aquifer and B. loosing stream, stream leaking to aquifer. Modified from Barlow and Leake, 2012

1.1.4.3. Well Boundary

Water is abstracted from the aquifer for agricultural use through high capacity irrigation wells. Irrigation wells in a groundwater model represent an interface through which the groundwater system loses some water with a given rate. During well operation, pumping drives groundwater flow towards wells to satisfy the pumping rate specified for the stress period for as long as water is available. In this model, wells are simulated using the USGS WEL6 package

(Langevin et al., 2017). In the Newton-Raphson formulation of the well package (used in this model to prevent drying cell conditions in case of relative excessive pumping), an optional automatic reduction was activated. The adjusted pumping rate is given as

$$Q_{wel} = S_{wel} \cdot Q_{wel}^{0} \tag{4-7}$$

where, Q_{wel} is the calculated pumping rate as a result of the reduction $\left[L^3/T\right]$, Q_{wel}^{0} is the specified pumping rate $\left[L^3/T\right]$. and S_{wel} the fraction of specified pumping rate $[-]$ defined as follows:

$$\begin{aligned} S_{wel(i)} &= \Delta v_i^{\,2}\left(\frac{-2}{\zeta_i^3}\Delta v_i + \frac{3}{\zeta_i^2}\right), 0 < \Delta v_i < \zeta_i \\ S_{wel(i)} &= 1,\ \Delta v_i > \zeta_i \\ S_{wel(i)} &= 0,\ \Delta v_i \le 0 \end{aligned} \tag{4-8}$$

with Δv_i being the height of the face through which flow occurs and $\zeta_i = \Phi \cdot L_{screen}$. Φ $[-]$ ranges between 0 and 1 and L_{screen} $[L]$ is the length of the well screen.

As pumping continues and flow is directed to the well screen, we can assess the potential change in discharge with respect to hydraulic head. When the flow reduction is applied with the Newton-Raphson formulation, the derivative of Equation 4-7 when $S_{wel(i)}$ is substituted by its corresponding expression from Equation 4-8 becomes

$$\begin{aligned} \frac{\partial Q_{wel}}{\partial h} &= Q_{wel}^{0}\left(\frac{-2}{\zeta_i^3}\ \Delta v_i^2 + \frac{3}{\zeta_i^2}\ \Delta v_i\right),\ 0 < \Delta v_i < \zeta_i \\ \frac{\partial Q_{wel}}{\partial h} &= 0,\ \Delta v_i > \zeta_i \end{aligned} \tag{4-9}$$

$$\frac{\partial Q_{wel}}{\partial h} = 0,\ \Delta v_i \le 0$$

The well package for this model is a text file that is read from the name file (see fc.nam and fc.wel in Appendix F) and which specifies the total number of wells (*MAXBOUND*) in the *DIMENSIONS* block as 482 and the information for all active wells for each stress period in the period blocks. The information for each well includes the model layer from which the well is pumping (*Layer*), the number associated with the cell in 2-D discretization (*cell2D*), and the volumetric pumping rate (Q_{wel}^{0}). The model uses a total of 482 wells across the entire modeling time span, but it is convenient to note that not all wells are active all the time. Each well is subject to start and end dates, that are used to determine well activity for each of the 75 stress periods when pumping is activated.

1.1.4.4. Recharge

Groundwater recharge, also known as deep percolation, refers to water that reaches the water table as a replenishment. In this area groundwater is recharged through (1) precipitation infiltration and (2) irrigation return, which is part of irrigation inefficiencies. Recharge, as applied to a groundwater model cell i is defined as

$$Q_{rch(i)} = I_i \cdot M_i \cdot A_i \qquad (4\text{-}10)$$

where:

$Q_{rch(i)}$ is the recharge flow rate applied to model cell i $\left[\ L^3/T\ \right]$,

I_i is the recharge flux applicable to cell i $\left[\ L/T\ \right]$

M_i is a dimensionless area multiplier that can be used to scale the flux $[-]$, to reflect conditions in low or high recharge zone

A_i is the surface area of cell i $\left[L^2 \right]$

The volumetric recharge rate for the whole model area with *NCPL*=19690 cells (see discretization package) and for stress period *sp* is given below.

$$Q_{rch(tot,\,sp)} = \sum_{i=1}^{NCPL} \left(I_i \cdot M_i \cdot A_i \right) \tag{4-11}$$

A value of recharge flux for each model cell is read from ASCII arrays for each stress period. Those values are outputs from a previously published Soil-Water -Balance (SWB) model (Westenbroek et al., 2010), used for the Northern High Plains aquifer by Peterson et al. (2016)

1.1.4.5. Evapotranspiration

Evapotranspiration (ET) represents the second largest outflow from the groundwater after irrigation. It is an interface whereby the groundwater system loses water through direct evaporation and plant transpiration. The GW model only simulates GW fed ET which does not include moisture abstracted by plant roots above the water table or pan evaporation on surface water bodies that are not hydraulically connected to the GW system. The MODFLOW ET package simulates ET discharge on the assumption that maximum ET applies when the water table reaches a predefined ET surface. Simulated rates of ET gradually decreases as water table drops and are completely cut off with water level below specified plant root extinction depth.

1.9 Groundwater Flow Model Discretization

In the control volume finite difference formulation shown in Equation 3-1, two of the most important variables are spatial discretization and temporal discretization. Spatial discretization in Equation 3-3 is represented by DR_j, DC_i, and $DV_{i,j,k}$ which are the cell dimensions in x, y, and z directions respectively. Temporal discretization is represented by the

duration of a time step, $t^{m+1} - t^m$. The next two sections describe the spatial discretization and temporal discretization that we used in this study.

1.1.5. Spatial Discretization

MODFLOW-6 supports three different types of spatial discretization including the structured discretization (DIS), the unstructured discretization (DISU), and the discretization with vertices (DISV) which is the newest type and is only supported by MODFLOW-6 within the MODFLOW family. Only one discretization package can be specified for a groundwater flow model. This groundwater model was discretized using DISV. The DISV package requires the user to specify a list of two-dimensional x, y vertex pairs, and for each two-dimensional cell, a number of defining parameters are specified in subsequent blocks. A DISV grid can have more than one layer but it is important to note that each layer is defined by the same two-dimensional discretization. The same number of cells found in layer one will be found in every other layer. Cells can be connected to other cells in both vertical and horizontal direction, but a cell can only be connected to one overlying cell and one underlying cell in the vertical direction. This groundwater flow model only has one layer, therefore there is no vertical connection between cells. However, given the choice of Voronoi grid discretization cells are polygonal with varying number of edges.A cell can be connected to a number of cells equal to or less than the number of edges. For a cell to be connected to another, they must share an edge. An edge is a line segment between two vertices. The DISV package is constructed with many blocks, each listing specific data. The *OPTIONS* block specifies that the unit of length is meter. The *DIMENSIONS* block of the DISV package for this model gives information for the grid dimensions

NLAY is the number of layers in the model $[-]$. $NLAY = 1$

NCPL is the number of cells per layer (19690) $[-]$.

NVERT is the number of (x, y) vertex pairs that is used to characterize the horizontal configuration of the model grid $[-]$.

The *GRIDDATA* block provides the following information for each of the 19690 cells.

TOP is top elevation with reference to a common datum for each model cell $[L]$.

BOTM is bottom elevation with reference to the datum for each model cell $[L]$.

IDOMAIN is an optional array that characterizes the existence of cell. If 0 is specified for a given cell, then the model does not compute a solution for it. In this model, all cells listed in the discretization package are active and therefore, the *IDOMAIN* would be an array of *NCPL* entries of ones. MODFLOW-6 also gives the option of using "*CONSTANT*" command followed by the desired value. Therefore, we've used that option instead of repeating 19690 times the number 1.

The next block in the DISV package is the *VERTICES* block which gives the following information

iv, the vertex number. Records in the block must be listed in consecutive order from 1 to *NVERT*

xv, the x-coordinate of the vertex

yv, the y-coordinate of the vertex

The next block in the DISV package is the *CELL2D* block and gives information pertaining to the two-dimensional configuration of cells within the layer.

icell2d is the cell2d number listed in consecutive order from 1 to *NCPL*

xc is the x-coordinate for the cell center.

yc is the y-coordinate for the cell center.

ncvert is the number of vertices required to define the cell. In this Voronoi grid, cells are polygonal with a varying number of sides and thus there may be a different number of vertices for each cell.

icvert is an array of integer values containing vertex numbers used to define a cell. Vertices defining a given cell must be given in a clockwise order. Cells that are connected share at least two vertices which define the surface through which flow across the two cells occurs.

In this DISV package, information about cell top elevation, bottom elevation, vertices, and cell2d are read from other text files using command OPEN/CLOSE followed by complete file path.

1.1.6. Temporal Discretization

Temporal discretization refers to the time component of the finite difference formulation of the groundwater flow model. Change in head for a given cell is computed at two different times t^m and t^{m+1}. The approximation for the time derivative of head is $\Delta h_n / \Delta t$. Figure 4-3 shows an example of hydrograph of head values changing through time step t^m, time step t^{m+1} and beyond.

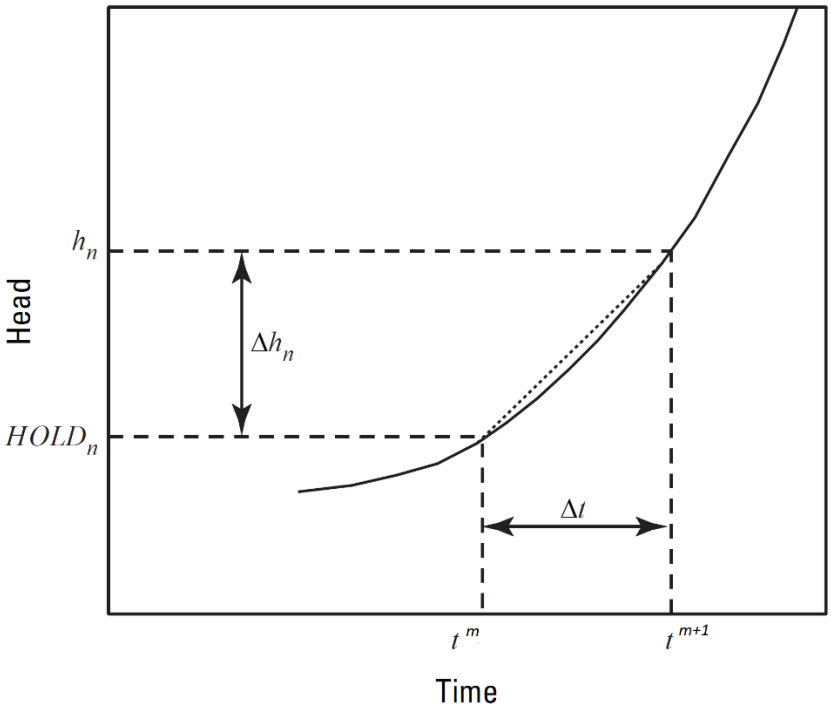

Figure 4-3: Hydrograph for n-th cell showing change in head from one time step to the next. Figure modified from Harbaugh (2005)

Typically, the change in head for the cell is found by integrating the head function in the given time interval through

$$\int_{t^m}^{t^{m+1}} \frac{dh}{dt} \tag{4-12}$$

The finite difference approximation to the time derivative of head is given by

$$\frac{\Delta h_n}{\Delta t} \approx \frac{h_n - HOLD_n}{t^{m+1} - t^m} \tag{4-13}$$

The TDIS package for MODFLOW-6 is a text file specified in the fmsim.nam file and defines the time unit, the model start date and time, the number of stress periods as well as the duration and number of time steps in each stress period. The *OPTIONS* block specifies the time unit and

the model run start date. The DIMENSIONS block provides *NPER*, the number of stress periods. The *PERIODDATA* block gives the number of time units composed in each stress period and the number of time steps.

This model uses days as time unit. The entire simulation period is discretized into 151 stress periods with varying lengths. We simulate two stress periods in a period of 12 months grouped in irrigation period and non-irrigation period. A typical irrigation period starts on May 1st of a given calendar year and ends on September 30th of the same year. This makes the irrigation period a 153-day long period. The non-irrigation period, on the other hand, starts on October 1st of a given year and ends on April 30th of the next calendar year. This makes the typical non-irrigation period a 213 or 212-day long period, depending on whether it is a leap year or not. An exception is given to the first and last stress periods to constrain the modeling period to the desired dates. Thus, the first stress period is a 120-day long period while the last stress period is 92 days long (see Appendix B).

1.10 Input Database

As for any numerical groundwater model, acquiring the correct input data is extremely important, but it also very challenging due to several limiting factors. Modeling historical conditions requires datasets that are sometimes unavailable or of poor quality. Groundwater level and stream discharge are very important input data used in model development as well as calibration targets. Unfortunately, in predevelopment and early development times, we did not have enough gages and observation wells in the study area. Most of the data collecting equipment that are found today in this study area have an operation starting date that is well after 1941. Data discontinuity was also encountered and sometimes required some correction strategies to fill in the gaps.

1.1.7. Well Data

Well data was necessary in building the well package, used by MODFLOW to simulate groundwater abstraction for agricultural use during the growing season. A database of well location and yearly pumping data was obtained from Traylor and Zlotnik (2016). This dataset was reported to have been collected from the Nebraska Department of Natural Resources online database (http://dnrdata.dnr.ne.gov/wellscs/Menu.aspx as reported in Traylor (2012)). Complimentary data such as well geographic coordinates, pumping start and end dates, screen depth, and well status were recently retrieved from https://dnr.nebraska.gov/data/groundwater-data for a total of 482 wells. Cumulative number of wells for each year from 1941 to 2015 (Figure 4-4) shows that many irrigation wells were constructed between 1970 and 1980. GIS data management tools were used to select wells within the groundwater basin. Figure 4-5 shows the spatial distribution of irrigation wells within the groundwater basin.

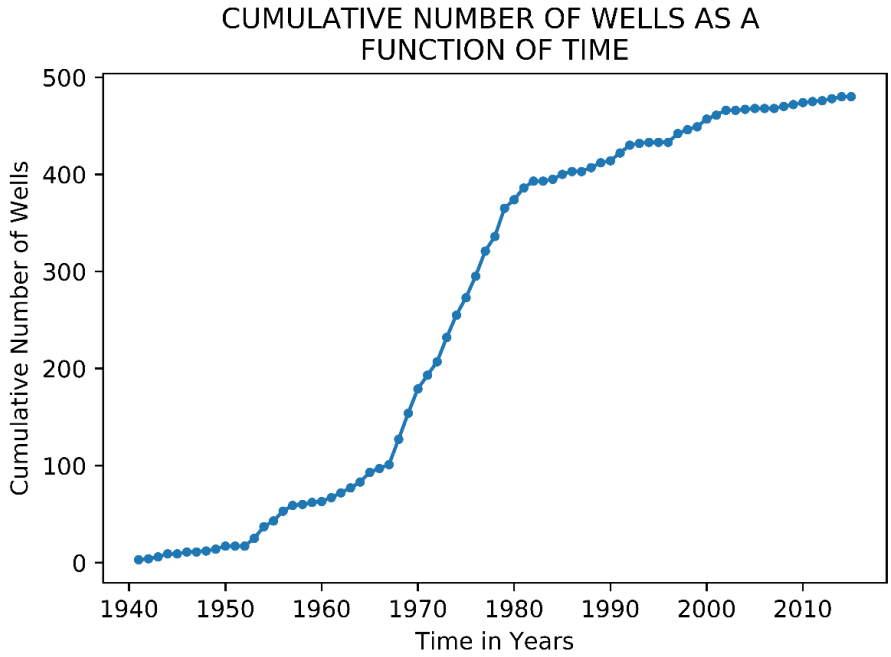

Figure 4-4: Cumulative number of wells in the study area as a function of time.

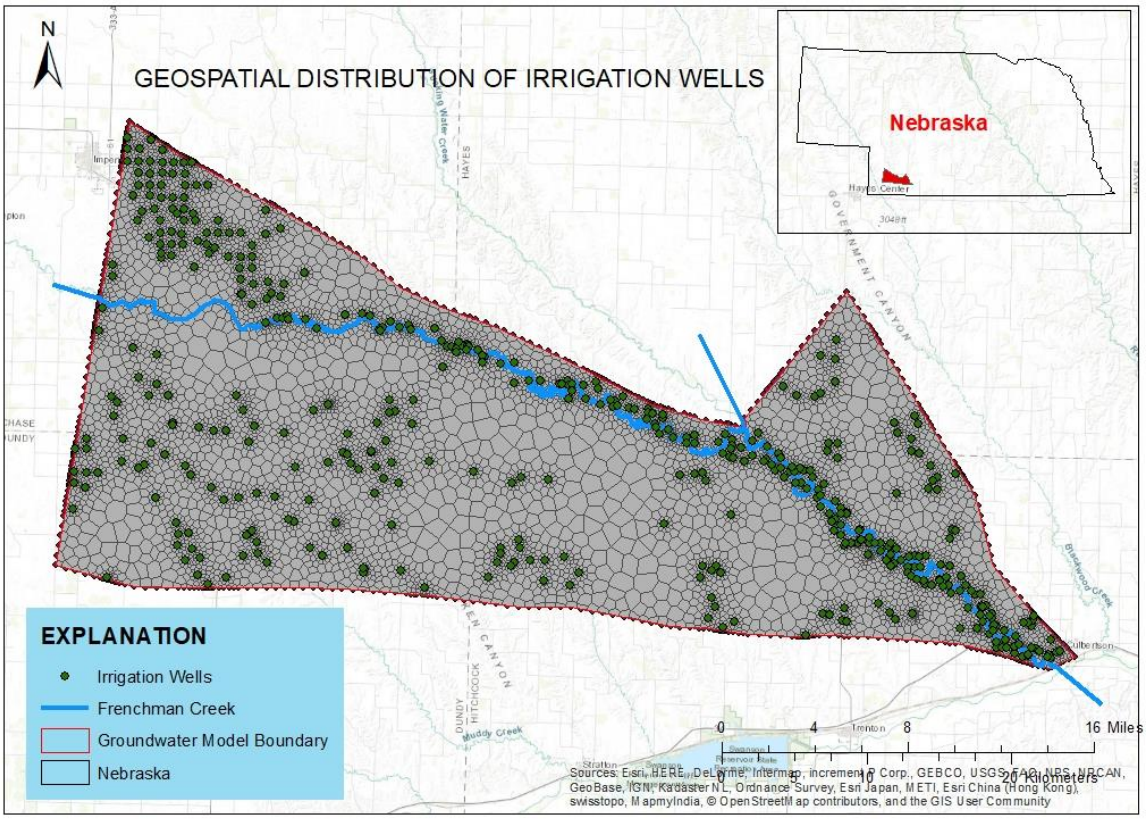

Figure 4-5: Spatial location of irrigation wells.

Using "Near" geospatial analysis coverage tool in ArcGIS, we computed the distance from each well to the stream and plotted the cumulative number of wells as a function of distance to stream (Figure 4-6). The plot shows that 50% of the wells are within 2.5 km from the stream.

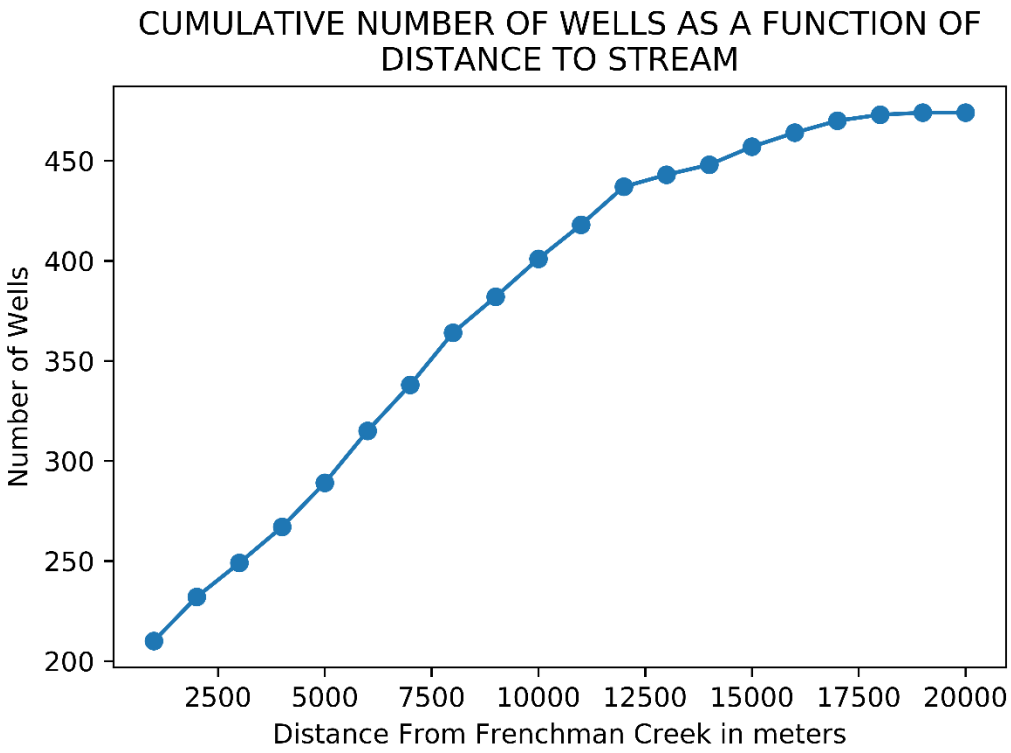

Figure 4-6: Cumulative number of irrigation wells within specified distances from the stream. The graph shows that 50% of irrigation wells are within 2.5 km from Frenchman Creek

1.1.8. Irrigation Data

The Nebraska Department of Natural Resources (DNR) provided irrigation pumping data as total yearly pumped data per 1000 m x 1000 m grid cell. The yearly data really represent total volume abstracted during growing season months (May, June, July, August, and September). The 1000m x 1000m discretization is the one used in the Republican River Groundwater Model (RRGWM) (RRGWM Committee, 2003). The Nebraska DNR used various data collection methods including metering wells or recoding fuel consumption for electricity production that was later used to calculate the corresponding pumped volume. In this modeling effort, all active wells for a given year are assumed to be pumping at the same rate. This approximation is due to the fact that total volume pumped was given per year and not per well. Total volume of pumped

groundwater for the i-*th* year was divided by total number of active wells for that year (n_i) to obtain the volume that would have been pumped by each well. This value was divided by the duration in days of the growing season stress period (May through September) to find the daily pumping rate, directly usable as MODFLOW well package inputs. Volumetric pumping rates of groundwater per irrigation stress period is shown on Figure 4-7.

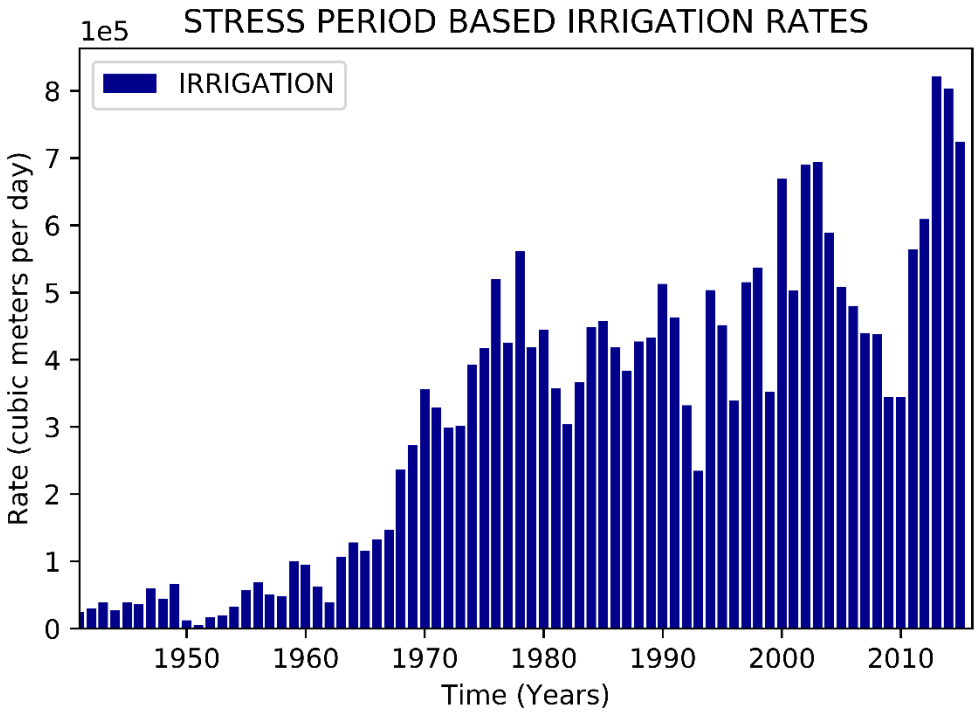

Figure 4-7. Groundwater irrigation rates estimated for irrigation period. Zero rate is applied during non-irrigation stress periods

1.1.9. Streamflow Data

Daily streamflow data were collected from both the USGS National Water Information System (NWIS) online surface water database (https://waterdata.usgs.gov/nwis/sw) and the Nebraska Department of Natural Resources database (https://dnr.nebraska.gov/data/surface-water-data). Streamflow data used as inflows to the model near Imperial were collected from the

USGS stream gage number 06831500 from 1941 to 1994 and from the NE-DNR and NWIS for the remainder of the modeling period (1994-2015). Data for inflows at Palisade were collected from the USGS stream gage number 06834500 from 1940 to 1950 and from USGS stream gage number 0683500 and NE-DNR for years 1949 to 1995 and 2005 to 2015. Data for stream discharge at Culbertson were collected from USGS stream gage number 06835500. Data for both Culbertson Canal and Riverside Canals were collected from the NE-DNR through personal communication with James Williams. The daily data were processed to meet the groundwater model temporal discretization requirements. That is calculating average for irrigation and non-irrigation stress periods from the daily discharge data, such that a single representative discharge rate is applied at inflows at Champions and Palisade. Figure 4-8 shows average streamflow by stress period for both FC at Imperial and SWC at Palisade. Outflows at Culbertson were also processed and used as calibration targets in parameter estimation.

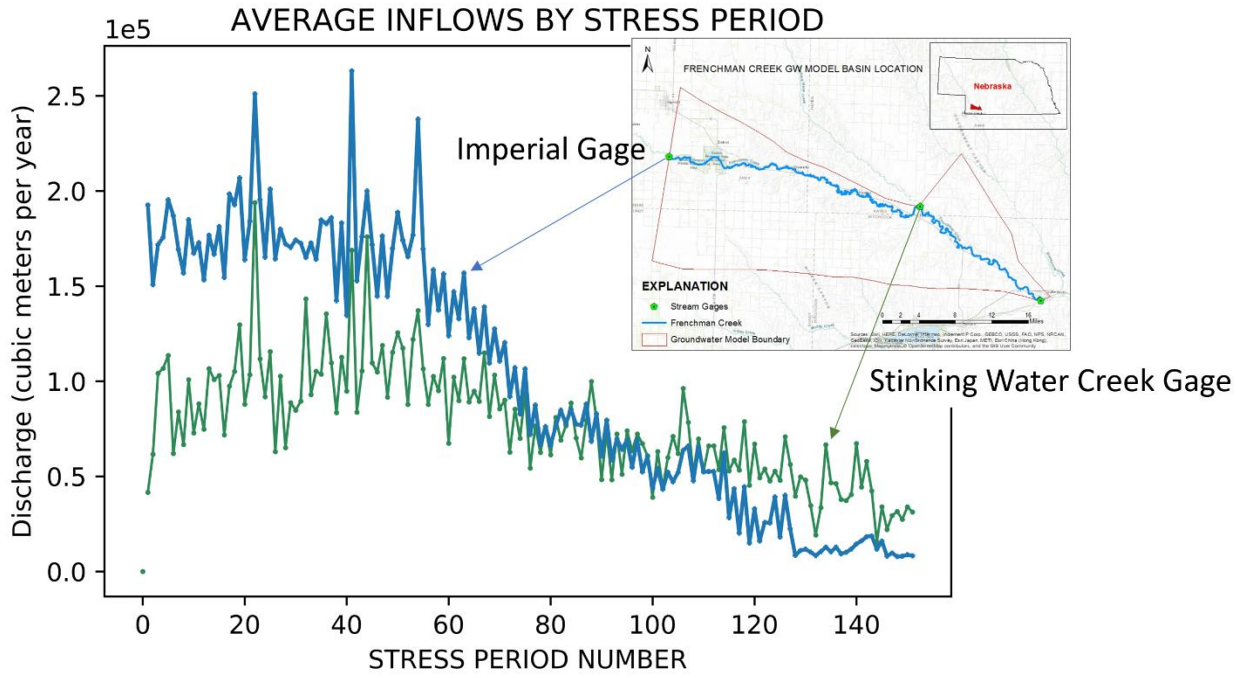

Figure 4-8: Average annual stream inflows to the model domain through Imperial and Stinking Water Creek gages. Inset map shows gages location

1.1.10. Soil Water Balance Related Inputs

1.1.10.1. Precipitation

Precipitation data is not a direct input to the groundwater model. They are rather used in conjunction with minimum and maximum temperature for developing the Soil Water Balance (SWB) (Westenbroek et al., 2010) model which is the means for proving both recharge and evapotranspiration data. The SWB model uses daily climate (precipitation, minimum and maximum daily temperatures) data along with land use and soil data to simulate groundwater recharge and evapotranspiration, which can be used directly in MODFLOW. The SWB model uses the Thornthwaite-Mather soil-moisture balance approach, common in analyses of the allocation of water in hydrologic systems, to determine the partitioning of infiltration into soil saturation and plant crop requirement. Figure 4-9 shows precipitation data from the National Oceanic and Atmospheric Administration (NOAA) weather station number GHCND:USC00254110 located at Imperial, NE.

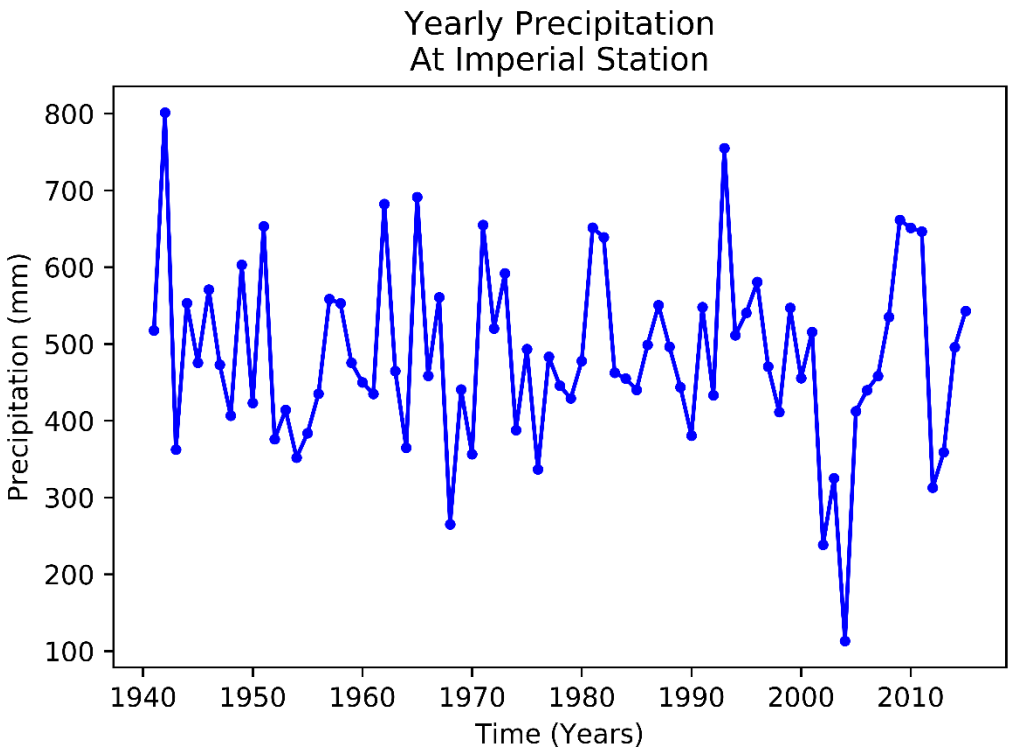

Figure 4-9. Annual precipitation record collected at the weather station at Imperial, NE (GHCND:USC00254110)

1.1.10.2. Recharge

Groundwater recharge data used in this model came from the outputs of the SWB model by Peterson et al. (2016). The SWB model code as conceived by Westenbroek et al., (2010) was based on a modified Thornthwaite-Mather soil-moisture balance approach to estimate spatial and temporal distribution of groundwater recharge. The code calculated recharge on a daily time step based on a variety of inputs including climate data, and outputs results as daily, monthly and yearly values as specified by the user. Groundwater recharge can be very dynamic and greatly vary over time. It is influenced by several parameters including but not limited to soil type which can cause it to be locally nullified. However, it is common for groundwater modelers to assume recharge to be a constant fraction of precipitation over time and space. The SWB code addresses

this issue very well and therefore it has been used in many studies (Dripps and Bradbury, 2001 and 2007; Stanton et al., 2011, Smith and Westenbroek, 2015, Peterson et al., 2016). Recharge data from the SWB model were processed and used to build the Recharge package for this groundwater flow model. Figure 4-10 shows the volumetric groundwater recharge rates by stress periods.

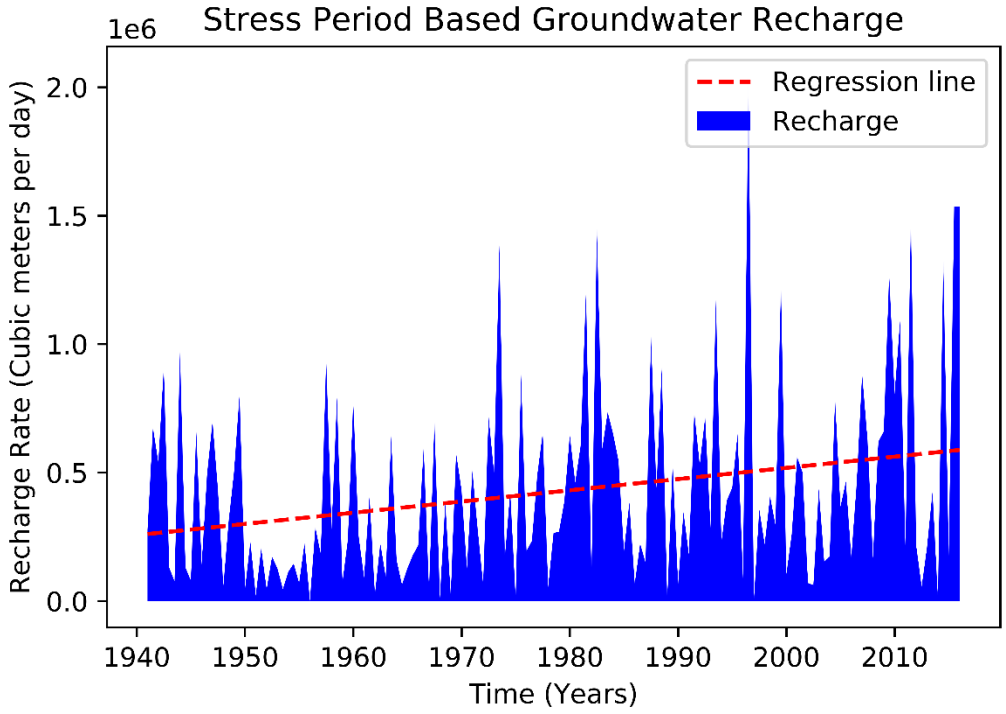

Figure 4-10: Groundwater recharge rates by stress periods. Regression line shows an increasing trend from 1941 to 2015

1.1.10.3. Land Use data

Land use is a required SWB input data, applicable to either static or dynamic conditions. For a static land cover, a single land cover scheme is specified, and the model uses it when it iterates through years. A dynamic land cover data includes seasonal or yearly changes. The SWB model that provided input data used in this study was built using a dynamic land cover (Peterson et al., 2016). Historical land cover data was collected from the FOREcasting SCEnarios (FORE-

SCE) of Land Use Change historical reconstruction by Sohl et al. (2007). In the land use gridded data, each model cell is represented by a single land cover for which a separate land use lookup table spells out its associated curve number, interception, maximum recharge, and root depth (Sohl et al., 2007). Each land use class is also associated with a specific crop coefficient used in the simulation of evapotranspiration. The effects of land use on the hydrologic cycle has been subject to numerous studies (Leopold, 1968, Bellot et al., 2001; Scanlon et al., 2005, Traylor and Zlotnik, 2016). It is, however, a consensus that the effects are still poorly understood, although many findings support the general idea that conversion of natural rangeland to agricultural ecosystems does increase groundwater recharge (Scanlon et al., 2005). In heavily irrigated areas such as FC basin, groundwater recharge has a precipitation component and an irrigation inefficiency component whereby a portion of groundwater abstracted by irrigation wells is not used by crops and ultimately infiltrates back to the aquifer as irrigation return flow (Traylor, 2012). Irrigation return flow coefficient is defined as the ratio between the quantity of water returned from the application field to the groundwater system from which pumping occurred. Irrigation return flow coefficients depend on irrigation technique, but they vary with crop type and are used to characterize irrigation efficiencies. Dewandel et al. (2008) reported that irrigation return flow coefficient can exceed 50% for rice when standing irrigation is applied but can also be as low as 0% in the case of drip irrigation techniques. One of the land use classes used by SWB model characterizes developed land cover, which includes cities and roads and has been expanding since settlement started. Developed areas are often covered with concrete and tar which increase runoff and decrease recharge substantially. These mixed effects of land use on groundwater recharge make it more difficult to understand from a water resources management

standpoint. The least we could say is that an effective groundwater flow model needs to be consistent with land cover types in the model domain and existing irrigation techniques.

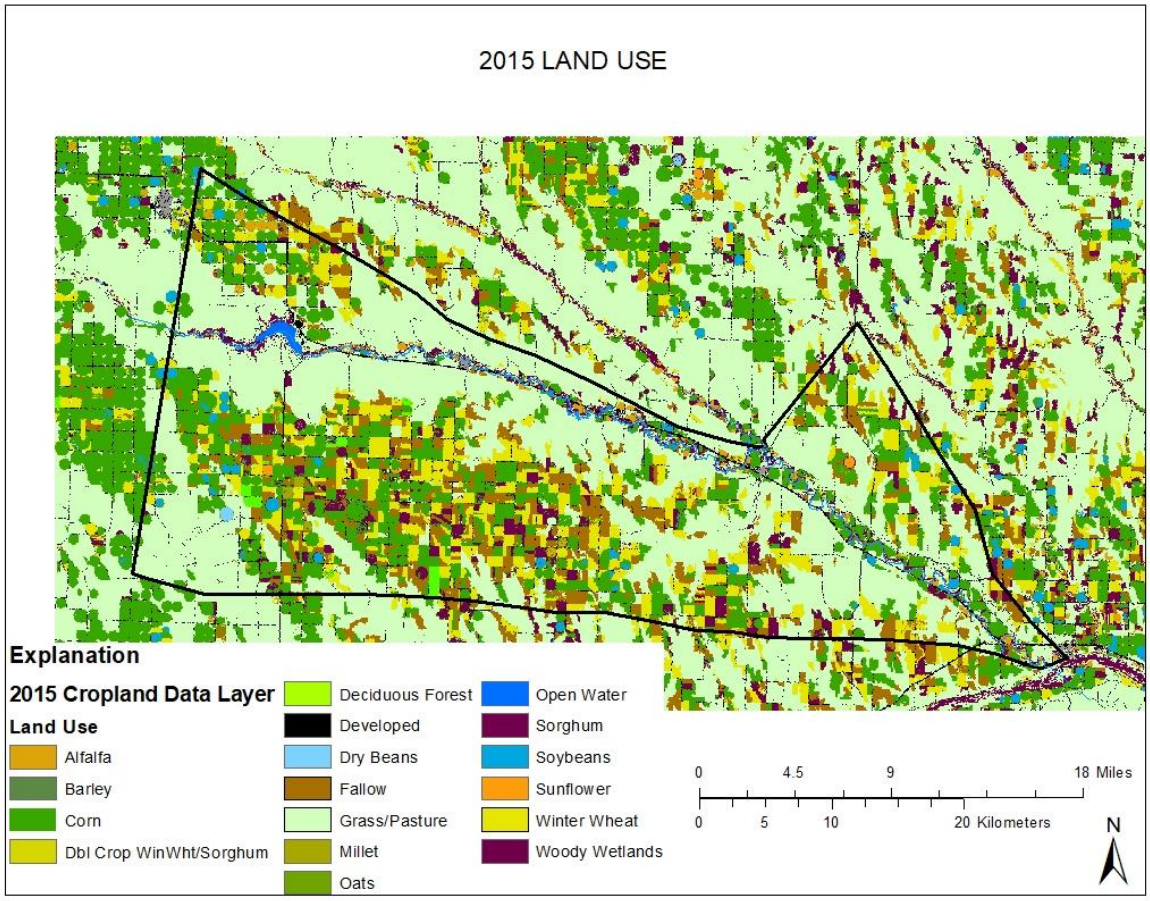

Figure 4-11: Land use in the study area in 2015. Data collected from the USDA Cropland Data Layer and processed in ArcMap

1.1.10.4. Evapotranspiration

Evapotranspiration (ET) is a hydrologic parameter that combines evaporation and transpiration. This occurs when the water table is close enough to the land surface to allow evaporation directly from the saturated zones and transpiration by plants whose roots reach it (Anderson et al., 2015). In this study, ET was simulated using the USGS's MODFLOW-6

supported ET package which requires potential ET value as input. Data used in this study as input potential ET were outputs from the SWB model. The SWB model is run separately from MODFLOW and can simulate potential and actual ET value based on the soil water balance. The simulated actual ET values do not represent discharge from groundwater but are results from a balanced compartmentalization of water inputs and outputs with respect to the soil. The potential ET values represent the maximum possible ET, which depends on other variables such as land use. The ET package assigns for each cell and stress period the following parameters: the maximum ET rate, the ET surface elevation, and the root extinction depth. Those values are supplied to MODFLOW for use in solving groundwater flow equation.

1.11 GIS Data Transformation

1.1.11. Datum And Projections

Data for this study were collected from various sources and come in a variety of formats. As a result, data processing was required for almost all original data to comply with one of the MODFLOW-6 supported data formats. Thus, some of the data were processed using ArcMap Geographical Information System (GIS) software. All GIS files such as shapefiles and raster files were brought to the same geographic and projected coordinate system to minimize errors in data processing such as raster resampling. North American Geographic Coordinate System (GCS_North_American_1983) and North American Datum (NAD_1983) were used. The Projected Coordinate System used was North American Datum Urchin Tracking Module Zone 14 for the Northern hemisphere (NAD_1983_UTM_Zone14N)

1.1.12. File Formats

MODFLOW-6 is a command line executable that reads input data from ASCII text files, and in some cases, when supported, from binary files. MODFLOW-6 also writes output files in

both ASCII and binary format. In this modeling effort, all input files were preprocessed and saved as ASCII files before they are read in by MODFLOW-6. Outputs however included ASCII text, binary, and comma separated files such as head and budget files. Post-processing of outputs included Python and ArcMap mxd files.

Model Calibration

1.12 Calibration Targets

Model calibration is the process by which required model parameters are iteratively adjusted until a satisfactory fit is attained between simulated values and field measurements (Moore and Doherty, 2006). Groundwater model calibration requires estimation of hydraulic properties throughout the entire model domain. The process involves testing values–within specified reasonable ranges–of parameters in order to find the best combination that would bring the model to replicate some observed values called calibration targets, which are very important in the calibration process. An uncertainty exists in calibration targets due to measurement errors; an observation value with a high uncertainty is weighted low in the priority list for the model to replicate. A total of 3427 observations in three observation groups were used as calibration targets. Observation groups include a baseflow group with 76 observations, a streamflow group with 151 observations, and a groundwater level group comprising 3200 observations. The table below shows observation groups with observation numbers along with the order of priority for the model to try and match during calibration.

Table 5-1:Summary of observations grouped by observation group, used in calibration of Frenchman Creek groundwater model

Observation group	Number of observations	Order of weight in calibration
Baseflow	76	1
Streamflow	151	3
Groundwater Levels	3200	2

Barlow et al., (2015) reported that separated baseflow values can be strongly influenced when irrigation wells are active. Therefore, baseflow separations used as calibration targets in this study only concerned non-growing seasons. During those times, there is little irrigation influence on GW-SW interactions and surface runoff is also limited. Streamflow and baseflow calibration targets are processed from daily discharge data to get a representative value for the stress period. Thus, an average value for daily discharge is calculated from data collected from May 1st to September 30st (5 months) of the same calendar year to represent the irrigation stress period for that year. The non-irrigation stress period for a given year is represented by the average from daily discharge data between October 1st of the previous year and April 30th (7 months) of the same year. Plotted calibration targets for baseflow to FC and stream discharge at Culbertson is shown on Figures 5-1 and 5-2 below.

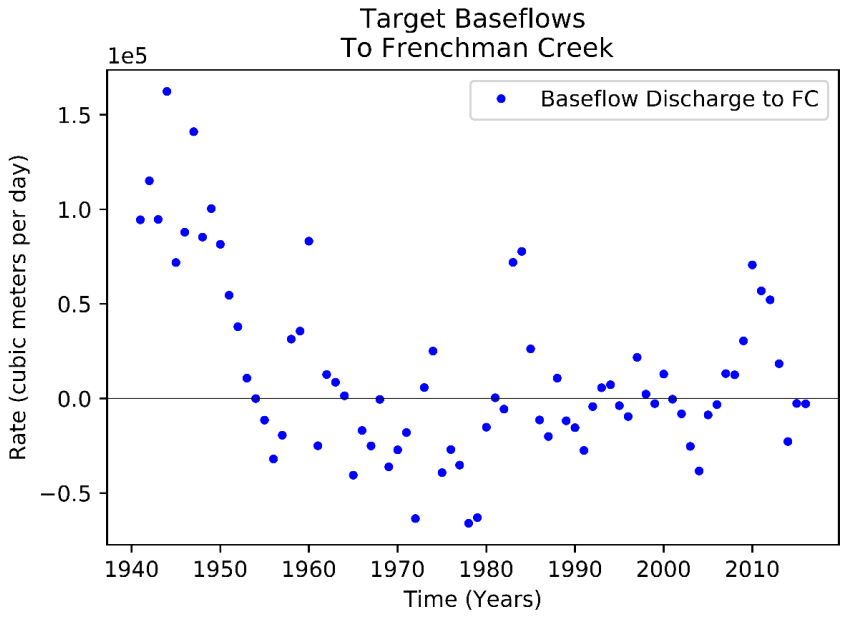

Figure 5-1:Target values for groundwater discharge as baseflow. All values below the zero line represent stream leakage.

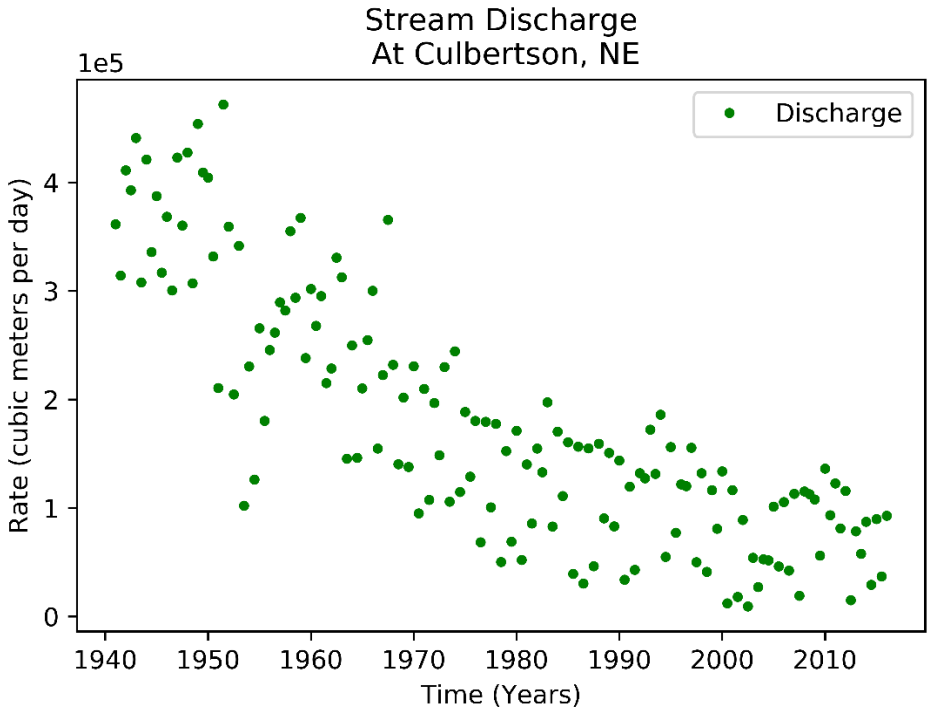

Figure 5-2:Stream discharge at Culbertson used as calibration targets

Besides baseflow and stream discharge at Culbertson, the model was calibrated against groundwater levels. Groundwater level measurement data were collected from 194 groundwater monitoring wells (see Figure 5-3) and processed to represent calibration targets. Unlike what was done with baseflow and discharge, groundwater level data were not averaged to produce one value representing the entire stress period. It is rather the value that is closest possible to the end date of the stress period with a five-day tolerance. That is, if there was no groundwater measurement record between April 25th and May 5th for a given year at a given location, then there is no calibration target for the non-irrigation stress period for that year at that specified location. The model does not have to work towards matching any specific head value at that location and time.

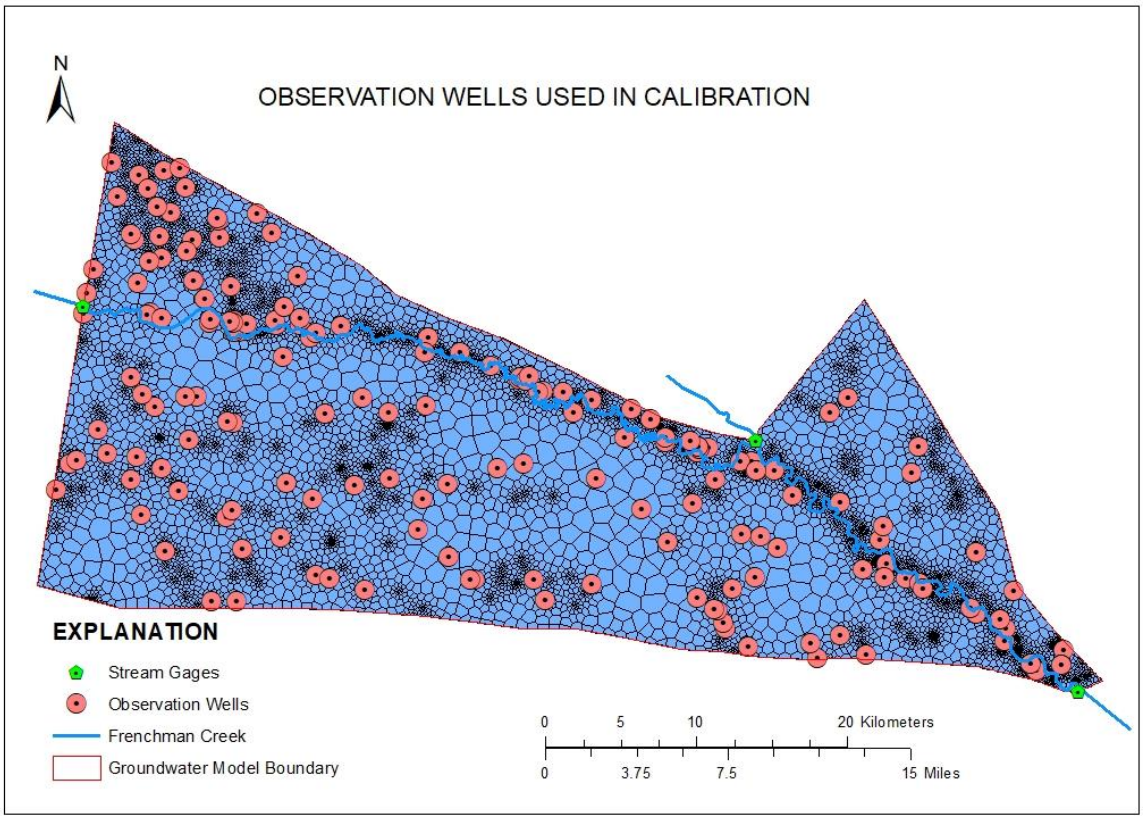

Figure 5-3: Observation wells where groundwater level data were used for model calibration

1.13 Calibration Parameters

1.1.13. Aquifer Hydraulic Conductivity

Hydraulic conductivity is one of the most important variables used in the groundwater flow analyses. It is used in computing transmissivity, which is a measure of rate at which groundwater flows horizontally through the aquifer.

Finding spatially distributed hydraulic properties for an entire model domain can be very challenging. Field techniques such as slug tests (Bouwer and Rice, 1976, Zlotnik, 1994), pumping tests (Kollet and Zlotnik, 2003), and laboratory experiments such as grain size analysis, constant head and falling head permeability tests have proven to be useful in approximating

hydraulic conductivity. However, significantly large differences in hydraulic conductivity values found using different methods have been reported. For example, Butler and Healey (1998) reported that on average, hydraulic conductivity values obtained through pumping test are considerably larger than estimated values from series of slug tests in the same geologic formation. Slug tests can be performed at many sites and still not be able to capture regional aquifer heterogeneity. Therefore, finding hydraulic properties for a groundwater model through model calibration is a very useful approach in the groundwater modeling process.

In this model, we define two zones with different hydraulic conductivity values based on aquifer material. Zone 1, which covers 84% of the model area is essentially composed of Ogallala Fm and Zone 2, the remaining 16% and which forms the FC River Valley is a quaternary alluvial deposit. The alluvial deposit comprises unconsolidated sand and gravel and therefore is of higher hydraulic conductivity compared to Zone 1 material. Figure 5-4 shows a map of the hydraulic conductivity zones.

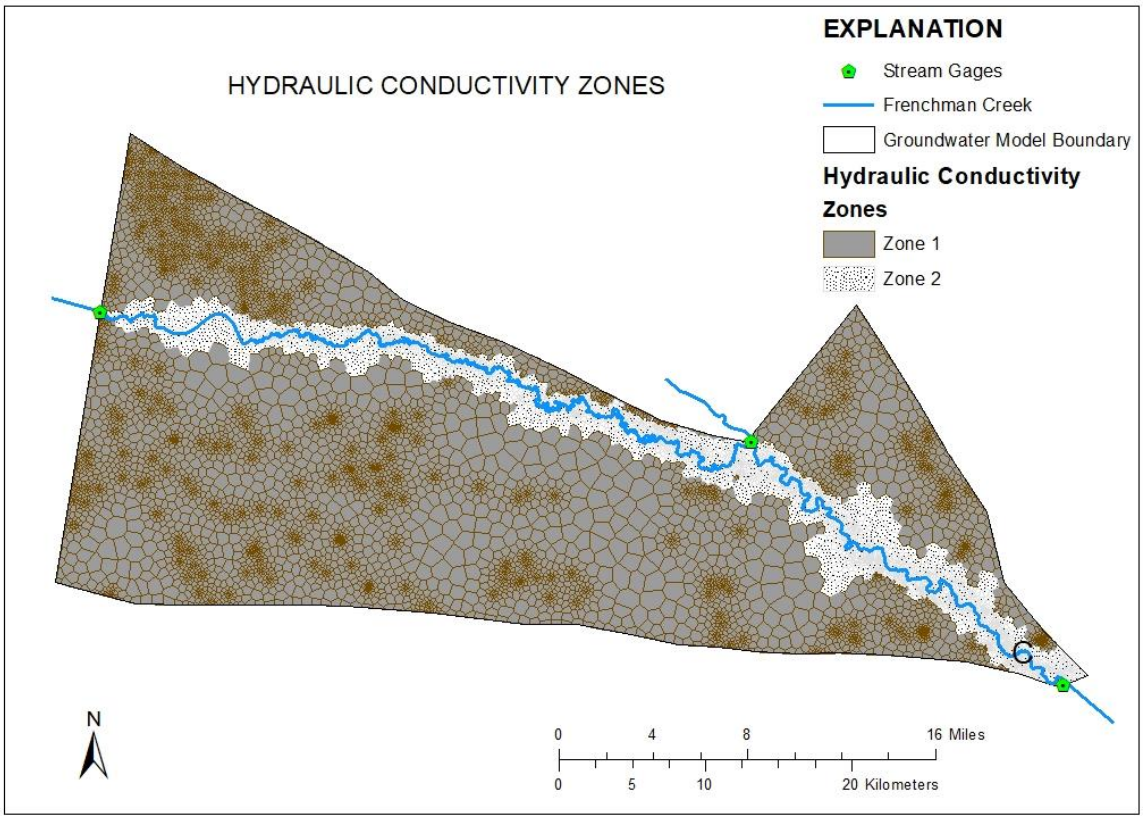

Figure 5-4: Hydraulic conductivity zones used in model calibration

1.1.14. Aquifer Storage

Storage coefficient or storativity is a dimensionless parameter defined as the volume of water released from storage per unit area of aquifer per unit decline in the water table (Freeze and Cherry, 1979). Water in subsurface bodies occupies pore spaces, so the maximum possible value for storativity is effective porosity. Storativity of unconfined aquifers is a quantity that is a function of aquifer thickness *b*, specific storage S_s, and specific yield S_y:

$$S = S_y + S_s \cdot b \tag{5-1}$$

In unconfined aquifers, the specific yield is generally orders of magnitude greater than the product of saturated thickness and specific storage, which makes the storage coefficient

heavily dependent on specific yield. In this model calibration, both specific yield and specific storage for each zone are parameters. The optimization process includes finding a good combination of those parameters

1.1.15. Streambed Conductivity

In Equation 4-6, groundwater discharge across streambed is given as function of streambed hydraulic conductivity. Streambed conductivity plays an important role in GW-SW interaction. Along with stream width and head gradient, streambed conductivity contributes in defining the rate of GW discharge to the stream as baseflow or SW seepage to the aquifer as stream leakage. Streambed conductivity was calibrated as a single parameter used for all stream segments.

Results And Discussion

1.14 Calibration Results

The objective of calibration was finding the best combination of parameter values that minimize differences between modeled outputs and field observation values. During calibration, the objective function value (Φ value) is minimized and the optimization process is monitored. Calibrated parameters were horizontal hydraulic conductivities, specific yield and specific storage for both zone 1 and 2 of the aquifer, and streambed hydraulic conductivity for FC. (Table 6-1).

Table 6-1: Calibration parameters and results

Parameter		**Calibrated Value**	
Aquifer			
Zone1	K_1	17.99	$m.d^{-1}$
	Ss_1	2.00E-05	m^{-1}
	Sy_1	0.14	[-]
Zone 2	K_2	28.52	$m.d^{-1}$
	Ss_2	8.17E-04	m^{-1}
	Sy_2	0.25	[-]
Stream			
Streambed Conductivity	K'	9.93	$m.d^{-1}$

Calibrated hydraulic conductivity values do support the hypothesis of two-zone aquifer heterogeneity. The more recent alluvial deposits in FC and SWC valleys have a higher hydraulic conductivity that the older material of Ogallala aquifer. Calibration was set up such that each of the hydraulic conductivity values could range within bounds between 1 m/d and 100 m/d. Previously reported hydraulic conductivity values in the area are within this interval. For example, calibrated hydraulic conductivity from the RRGWM (2003), which was used in an

analytical model by Traylor and Zlotnik (2016) was 10m/d while Traylor (2012) reported an average value of 14.9 m/d with a minimum of 5.2 m/d and a maximum value of 30.5 m/d. Lappala's (1978) report on the quantitative hydrogeology of the Upper Republican NRD shows that the geometric mean of hydraulic conductivity values from bore hole testing was 18.75 m/d (61.5 ft/d).

The hydraulic conductivity values reported in Table 6-1 are consistent with the values reported in previous studies. The final and optimized values did not reach the parameter bounds. This suggest that this parameter combination yields the best match. Specific storage values have not been reported by previous studies; the focus was rather geared toward specific yield, which, along with specific storage, defines storativity, also referred to as storage coefficient. Calibrated *Ss* values ranged between $2 \cdot 10^{-5}$ m^{-1} and $8.73 \cdot 10^{-4}$ m^{-1} for Ss_1 and Ss_2 respectively. Specific yield on the other hand was calibrated to relatively lower values as compared to previously reported values. Thus, our calibrated specific yield values are 0.14 and 0.25 for zone 1 and zone 2 respectively, while Traylor (2012) reported an average of 0.18. Calibrated streambed conductivity was 9.93 m/d which characterizes a good stream-aquifer connection.

1.15 Model Outputs

Calibrated parameters were used to perform a forward MODFLOW run, producing the outputs that are analyzed and discussed below.

1.1.16. Baseflow

In this modeling effort, the primary goal was to simulate baseflow. The groundwater abstraction by irrigation and land use-based changes create streamflow depletion because of the linkage between SW and GW. The interaction between the two water systems is the key process;

therefore, the model was built in an effort to simulate that interaction. Analysis of model outputs allows us to understand the extent to which changes in inputs affect variables of interest.

Model results show a good match between modeled and observed baseflow values (Figure 6-1). The model was able to replicate year to year variations along with long time trends. There was a generally decreasing trend in baseflow from 1941 to 1956 with a clearly pronounced steep slope. This trend was changed for the following four years of simulation, leading to an increase up until 1960. All values below the zero line represent stream leakage and are the results of when the combined loss from the stream segments is greater than gain. Both simulated and observed values show that FC first became an overall loosing stream in 1954. The number of wells within the basin increased from 25 in 1953 to 37, a 48% increase while precipitation records shows a drop from 414 mm in 1953 to 351mm, a 15% decrease. Results also show that FC, documented as a gaining stream (Lappala, 1978 and Peckenpaugh 1995) was more of a losing one between 1960 and 1990; a period when the number of wells increased by 587%.

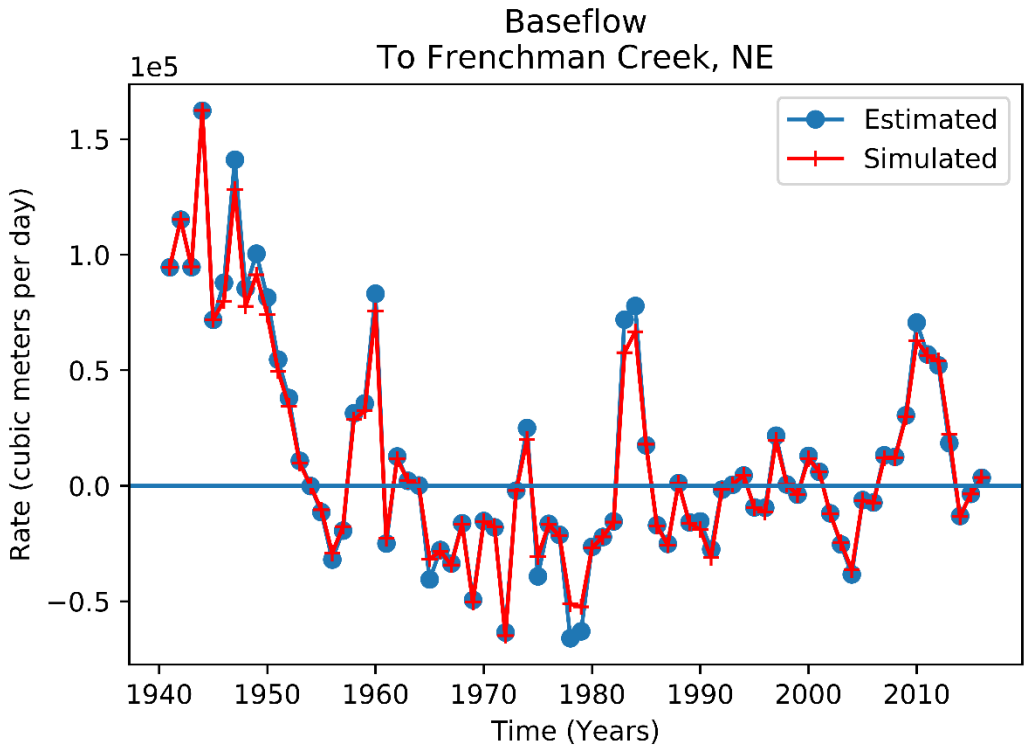

Figure 6-1: Simulated and Estimated baseflow after calibration. All values below the zero line represent stream leakage when the river is loosing water to the aquifer. Simulated values are net terms. Some segments of the river loose water while others gain as baseflow. The values plotted here are essentially absolute value of gains minus absolute value of loss.

1.1.17. Evapotranspiration From Groundwater Upward Flux

Model calibration yielded a set of parameters that minimized differences between simulated and observed values for ET from upward flux from the aquider. But besides calibration targets, other fluxes involved in the groundwater flow model are responsive when the model is run. Results show that simulated ET values are different from input ET values. Rates specified in the MODFLOW ET package were also associated with ET surface elevation and plant root extension depth. Seasonal variations observed on ET data (Figure 6-2) are consistent with weather changes and differential plant activities along stress periods. ET rates increase

during growing season and this is due to the fact that crops and other plants engage in in full photosynthesis process requiring more plant root uptake. High temperatures during summer months, not only drive plants to increase their root uptake to cool off internal circulatory system, but also increase pan evaporation from the open water. High ET rates are also linked to increased water use during photosynthesis and growth Relatively lower ET rates are observed during non-irrigation stress periods which stretch from October to April, including winter season with low temperatures. The long-term decline in ET is due to the drop in GW levels, because fewer plant roots reach the water table. Decadal average for total volume of GW discharge to ET during growing season dropped from $704,796 m^3$ in 1940s to $509,897 m^3$ in 2000s. The non-growing season values dropped from $516,597 m^3$ to $386,875 m^3$. In either case, discharge to ET dropped by about 25%.

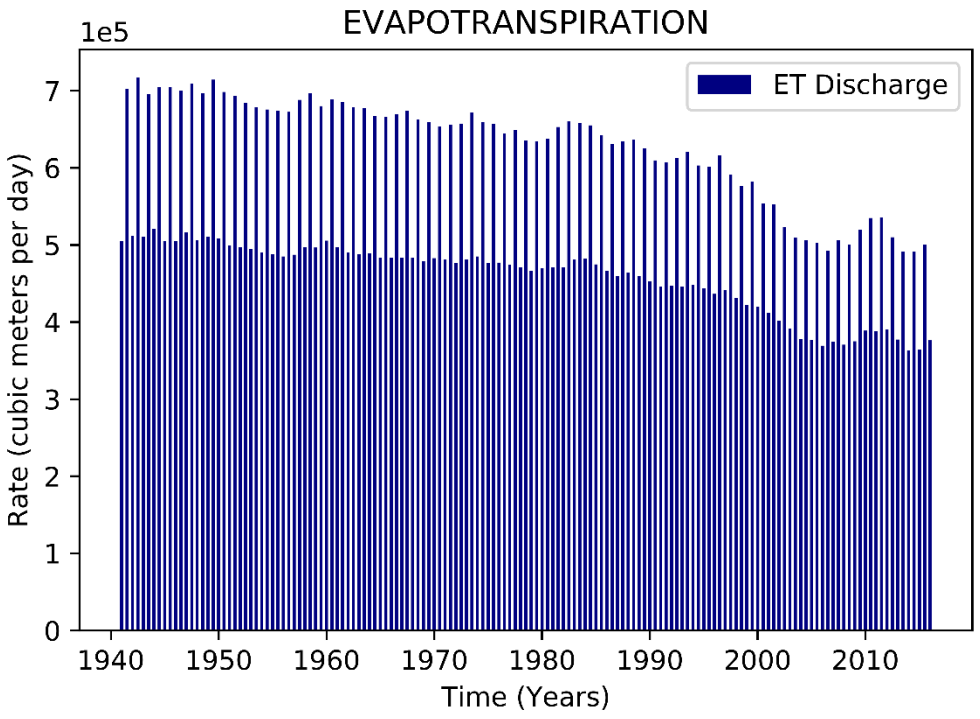

Figure 6-2: Groundwater discharge to evapotranspiration in disturbed condition

1.1.18. Groundwater Inflow

On the boundary that was set up for this model, there are two segments through which GW can flow into the domain. Both these segments are represented by prescribed head boundaries (AA' and BB' on Figure 4-1). As described in section 4.1.1, these head boundaries maintain GW levels at the prescribed values and designated time. As a result, when MODFLOW is run, flow is induced due to the hydraulic gradient that exists between the prescribed boundary and the reminder of active model cells. The amount of GW inflow for a given stress period not only depends on hydraulic gradient, it also depends on the saturated thickness. Thus, the long-term decline on GW levels is seen in inflows. Analysis of Figure 6-3 shows that the decadal average amount of GW flowing into the model domain has decreased by 56% from 1940 to 2000.

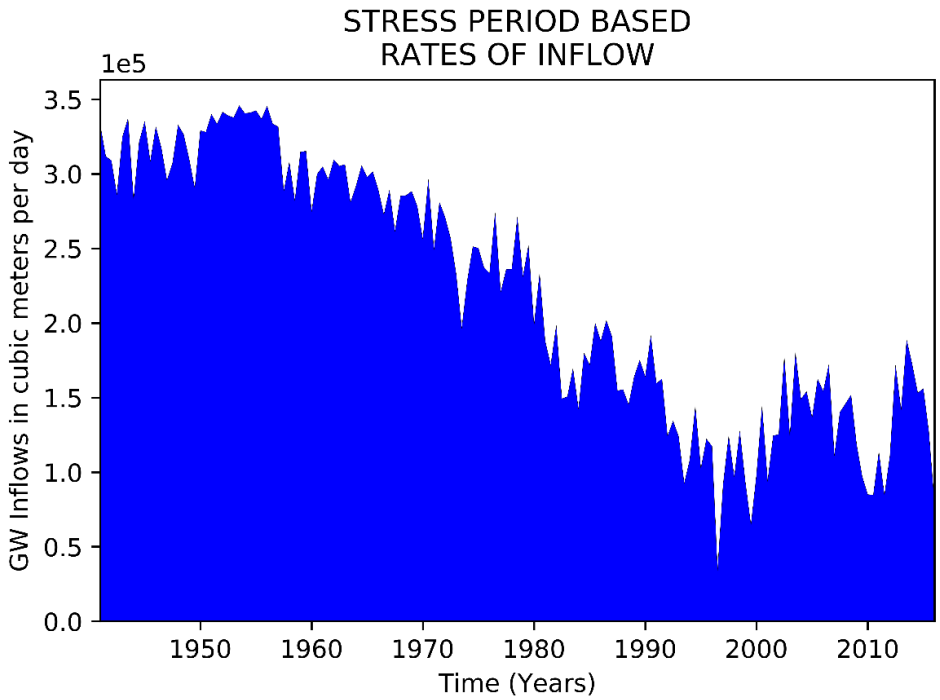

Figure 6-3: Declining groundwater inflow rates to model domain in disturbed condition due to long-term groundwater level and transmissivity decline at the boundary

1.1.19. Stream Outflows By Numerical Model

The model was also able to replicate seasonal variations as well as long term trends in model stream discharge at Culbertson (Figure 6-4): The decadal average has significantly decreased from more than 300.000 m^3d^{-1} in the years 1940s to about 70.000 m^3d^{-1} in the years 2000s. Analysis of the graph shows that simulated values are generally lower than the observed ones. However, the residuals between simulated and observed data have significantly decreased in the last 15 years of the simulation, and the model better represents more recent streamflow conditions than earlier ones.

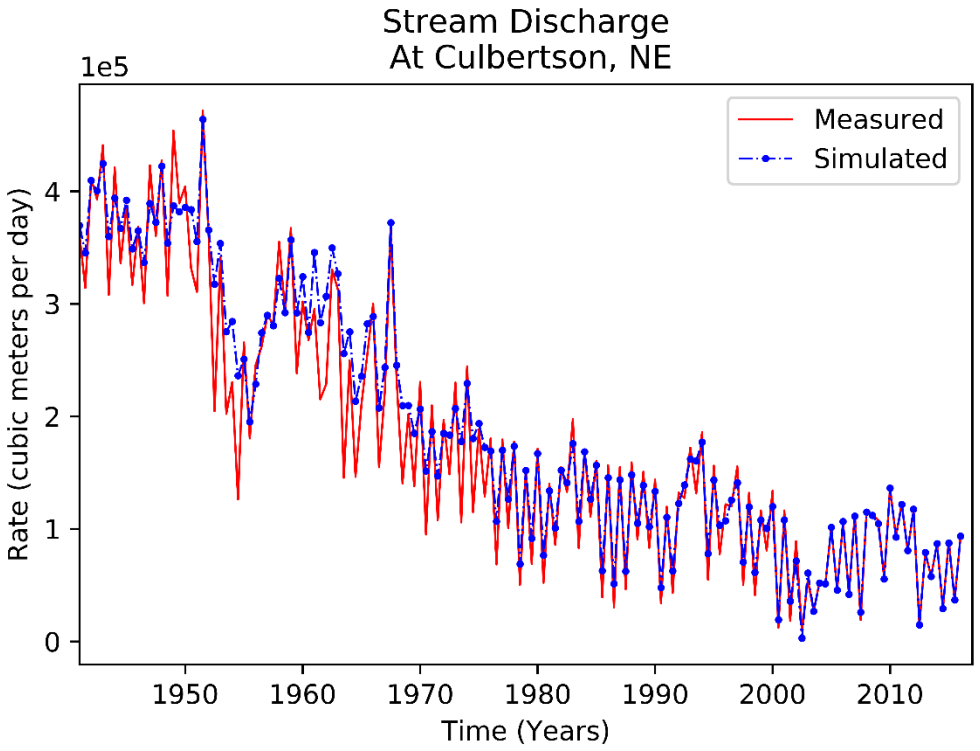

Figure 6-4: Simulated and measured stream discharge at Culbertson, NE

1.1.20. Comparison Of Disturbed And Base Condition

In order to better understand the effects of the changes within the study area over the last six and half decades (1950-2015), we investigated a hypothetical base condition that would have

been spared from anthropogenic influence on land use and well development. To do this, we ran a model using the same aquifer and stream property values found through calibration while maintaining GW abstraction rates and land use at values similar to those in 1948 (Figure 6-5) a time when GW development in the area was still very low. As a result, GW recharge and maximum ET rates from growing season 1948 were applied to subsequent growing seasons. Rates from non-growing season 1948 were also applied to subsequent non-growing seasons. Water levels used in prescribed boundary condition were also maintained at a higher value than those in disturbed condition.

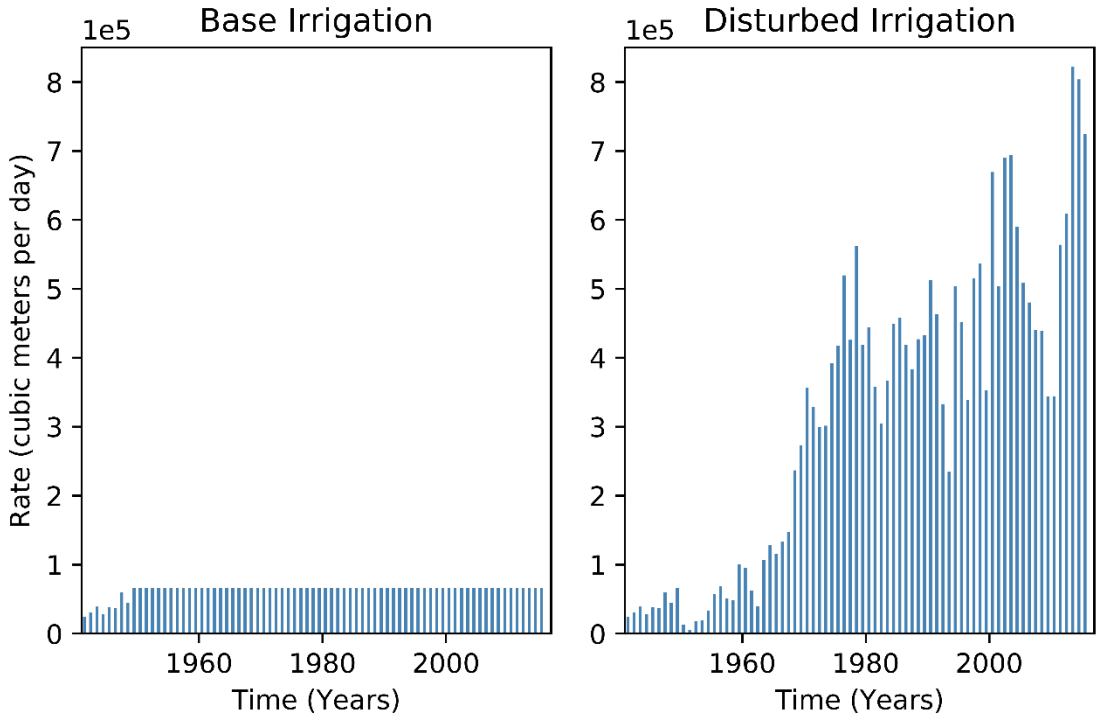

Figure 6-5: Groundwater irrigation rates applied to irrigation stress periods for base and disturbed conditions

The base run results were processed and plotted along with results from disturbed condition. Results show that GW discharge to ET in base condition starts out exactly as in

disturbed condition, but differences arise as pumping increases with disturbance (Figure 6-6). GW inflows to the model domain remain high for the entire simulation period in base condition (Figure 6-7) while a significant decline is observed in disturbed conditions. This is consistent with a higher transmissivity value when compared to disturbed condition where GW level decline affects saturated thickness and therefore transmissivity.

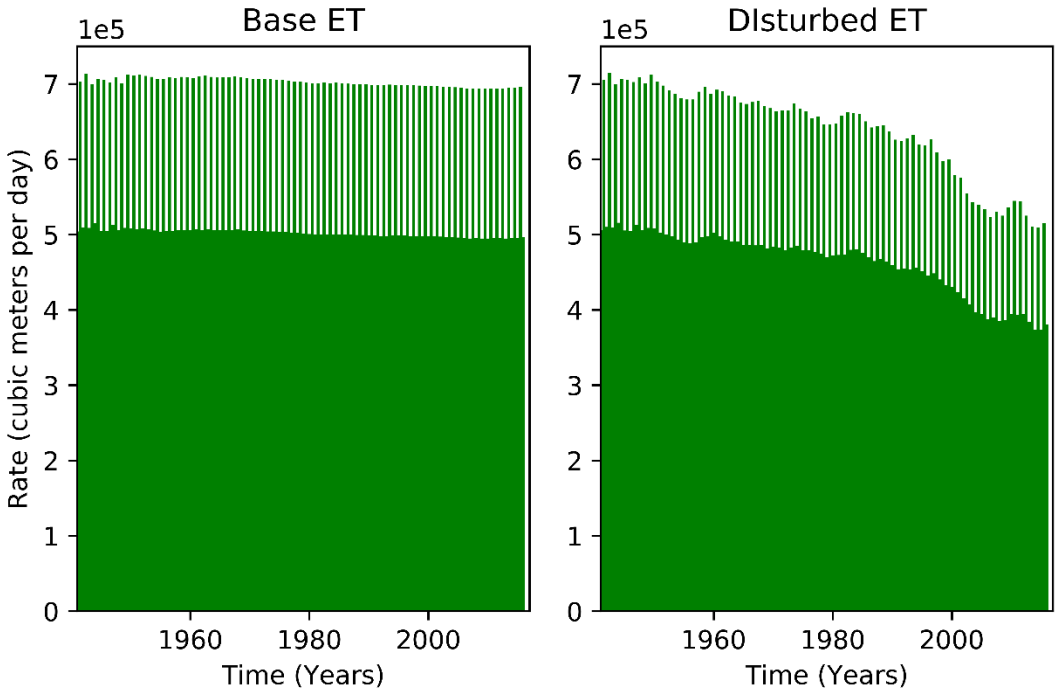

Figure 6-6: Base and disturbed conditions of simulated Groundwater discharge to ET

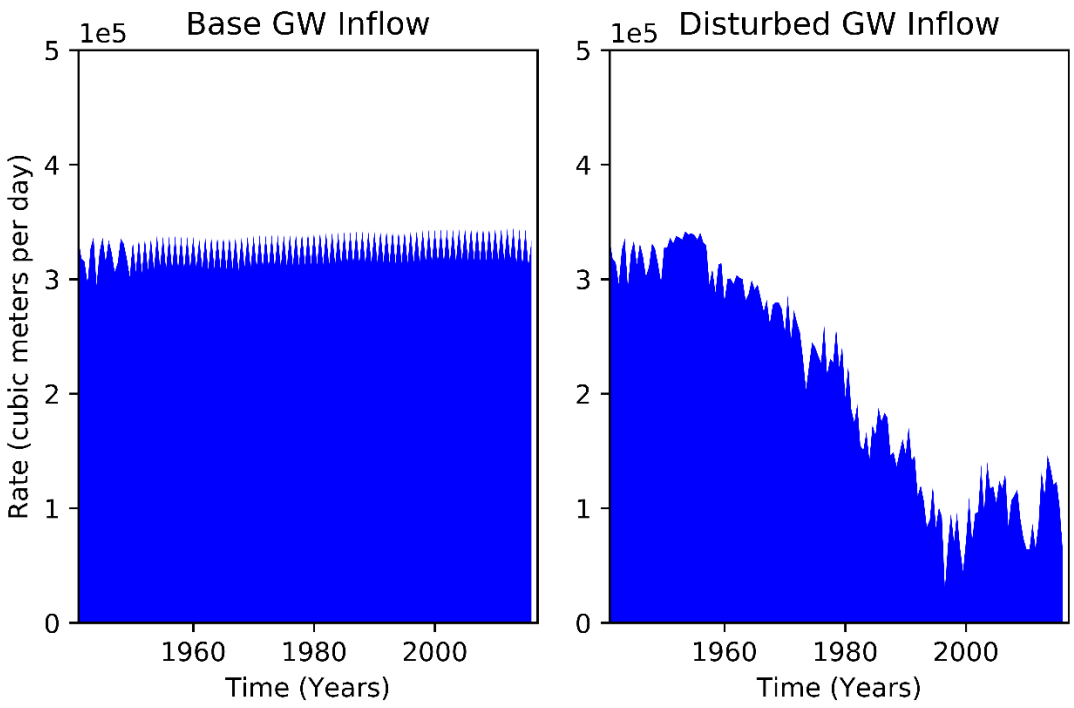

Figure 6-7: Base and disturbed condition of simulated groundwater inflow to model basin

It is also important to note that in base condition, FC almost stays in the same gaining regime where groundwater discharges to the stream as baseflow (Figure 6-8). Only in two of the 151 stress periods does FC switch to a losing regime with stream segments slightly leaking SW into the aquifer. In disturbed condition, FC is in losing conditions during 91 of the 151 stress periods.

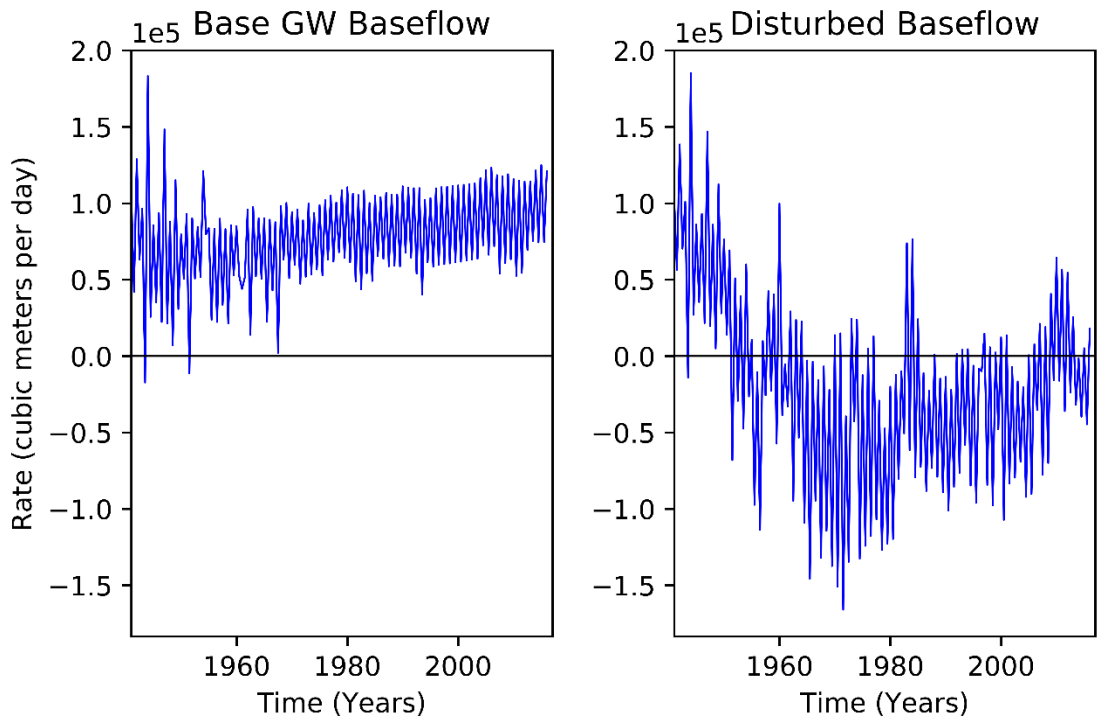

Figure 6-8: Base and disturbed conditions of GW discharge to stream as baseflow. All values below zero line are stream leakages

Analysis of changes in storage show that in base conditions, the cumulative effect of simulation time results in storage increase (Figure 6-9). However, in disturbed condition, the cumulative effects show that more water was released from storage despite the evidence that precipitation, and, more importantly, groundwater recharge has increased during the simulation period. Stream outflow at Culbertson in base condition does show a decreasing trend but discharge remains higher compared to simulated values in disturbed condition (Figure 6-10)

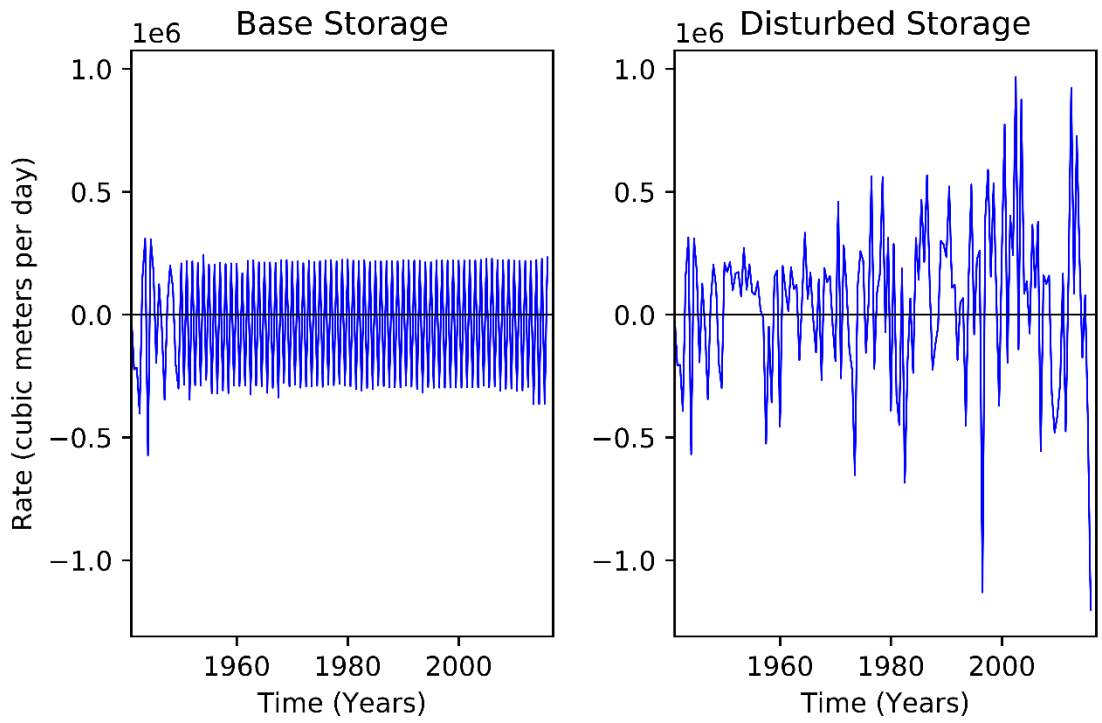

Figure 6-9: Base and disturbed condition changes in groundwater storage

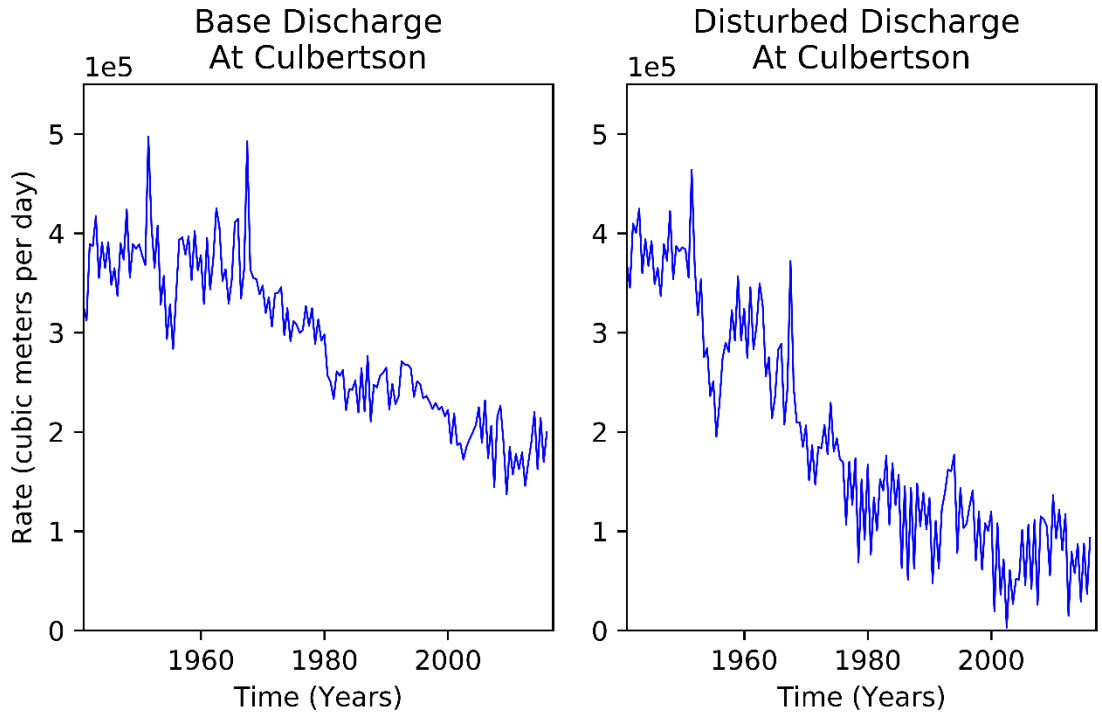

Figure 6-10: Base and disturbed conditions for stream outflow at Culbertson

1.16 Comparing Numerical Model To Analytical Model By Traylor And Zlotnik

An analytical model was constructed by Traylor and Zlotnik (2016) to study the effects of land use and irrigation on streamflow depletion in semi-arid conditions. The model was based on the same area location as in this study and ran from 1941 to 2009, which is 6 years shorter than in this study. The water budget components were evaluated on a yearly time step with no distinction between growing and non-growing seasons.

Temporal discretization in the analytical model and the numerical model differ. The time steps in numerical model were designed to capture seasonality of the major hydrological stresses. Growing season in this model domain in characterized by high capacity well operations that are very important in the hydrologic cycle. These operations result partially from a significant difference in precipitation received during this time as opposed to non-growing season. This refinement provides better fidelity of the model. However, differences in timing of model outputs requires a procedure for comparing results with analytical model. In addition, other stress factors are different. In order to mitigate this problem, data from numerical model are resampled using the following steps:

- We define a time variable $\tau(j)$ for numerical model such that $\tau(j) = 1 year$ in duration; *j* representing calendar year.
- $\tau(j)$ is a three-period sequence of *j*-th year, which consists of the 4 months (January through April) of non-irrigation season for, plus 5 months of irrigation season (May through September), and plus the 3 months (October through December) of post-irrigation season for year *j+1*.
- Numerical outflows are grouped to represent year *j* following $\tau(j)$ scheme

- Finally, simulated discharge for year *j* from analytical is compared to numerical data from the preceding step.

The diagram on Figure 6-11 shows time discretization of numerical model and how stream outflows are resampled using τ_j and τ_{j+1}, to facilitate comparison of analytical and numerical model, in addition to stream discharge.

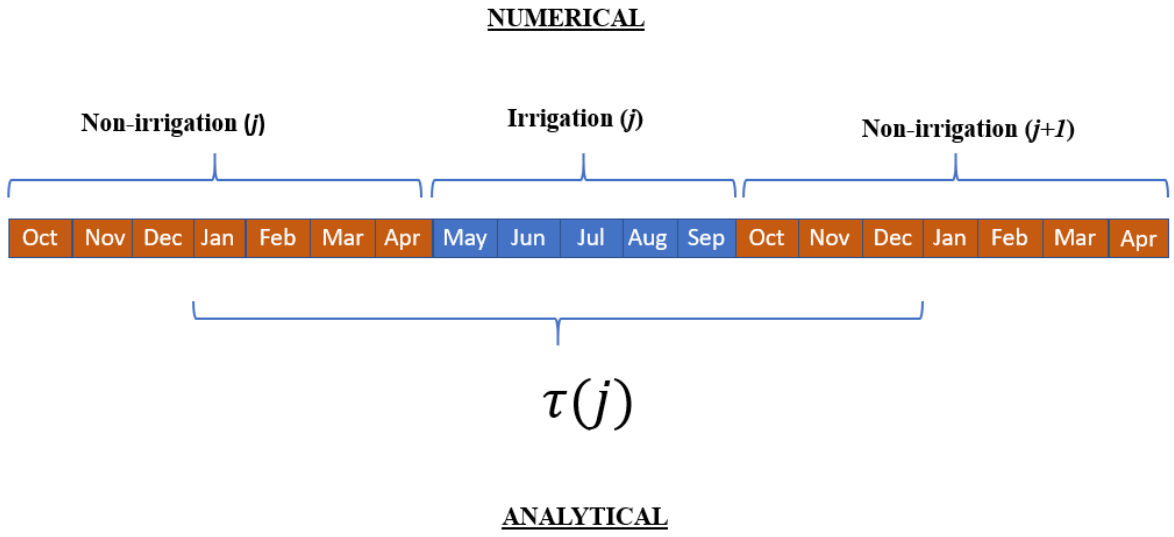

Figure 6-11: Relation of time steps of numerical and analytical models, when the stream discharge for j-th year in analytical model corresponds to three-segments of numerical model.

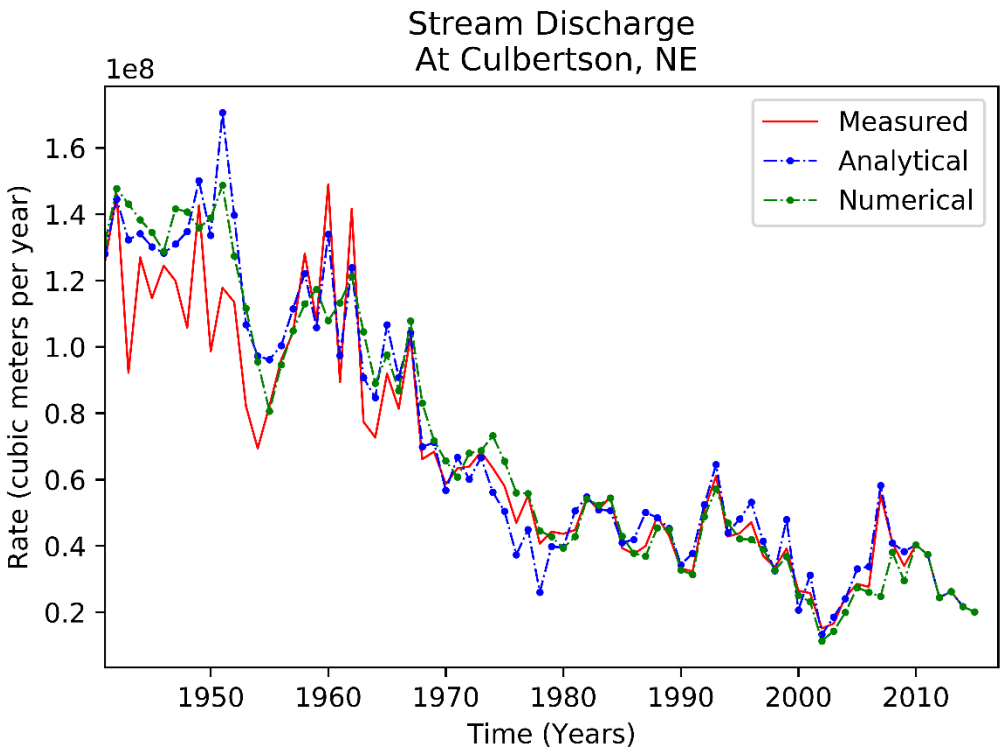

Figure 6-12: Measured, analytical, and resampled numerical model outputs

The diagram depicts a perfect scenario situation where resampling can be easily and accurately done along the lines of months. However, the numerical model is not discretized to match exact calendar months; input data for stress periods would also have been averaged using five or seven-month data depending on whether it is growing season.

Results from the numerical model have finer temporal resolution (time discretization) of stream discharge than the analytical model, and resampling (averaging) was needed for comparison with analytical model. Although the numerical model better captures majors variations found in field data, the analytical model offers a better approximation of annual discharge with maximum discrepancy of 44% while resampled numerical outputs has a maximum discrepancy of 65%.

The model was calibrated against baseflow observations primarily; therefore, any vetting or evaluation should include how well the model reproduces baseflow (Figure 6-13) A scatter plot of simulated versus observed baseflow values has an R^2 = 0.994.

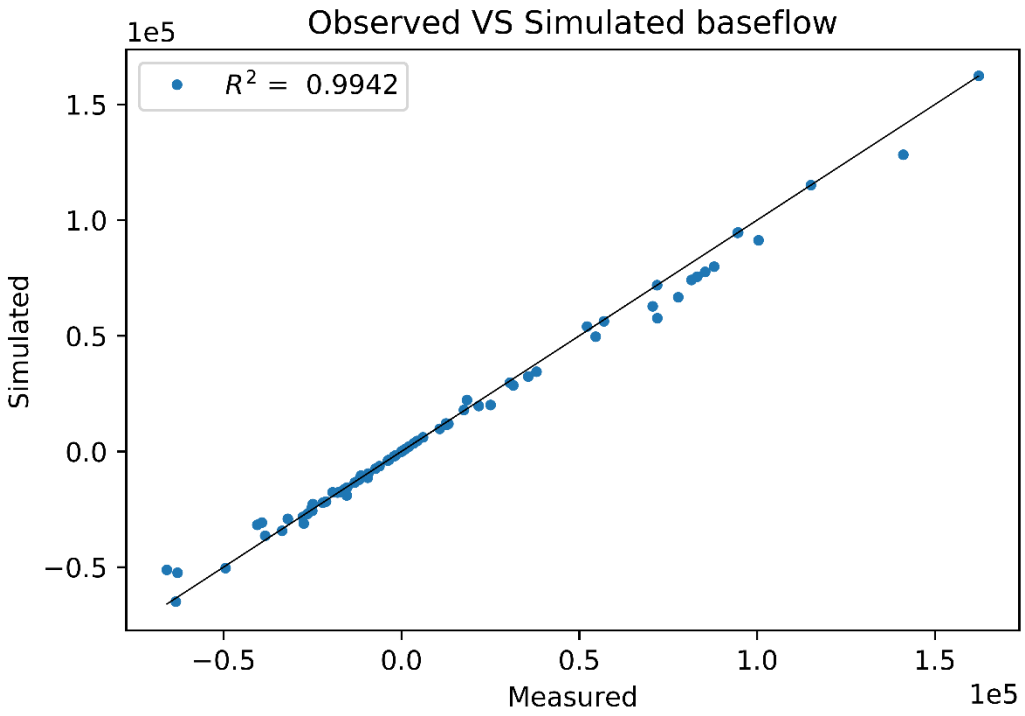

Figure 6-13: Simulated versus measured groundwater discharge as baseflow

Conclusions

This modeling effort was intended to build a tool using one of the latest resources available within the groundwater modeling practice for analyses of groundwater flow processes within FC basin under land use and irrigation changes. The choice of the method used in this study was partially motivated by the desire to address some of the limitations of the analytical model by Traylor and Zlotnik (2016), which was able to reproduce both baseflow and streamflow at Culbertson with small errors. This model is a tool that can be used by water resources management to test the effects changes in irrigation rates in select zones for better decision making. The use of numerical model allowed us to come to the following conclusions:

1. Change in transmissivity as a result of GW level decline, which was taken into account in transient prescribed head boundaries, reduced groundwater inflow to model domain by more than 50% from 1950s to 2015.
2. GW discharge to ET decreased by 25% from 1940 to 2015 due to water level decline despite a general increase in recharge. The decline lead to less plant root reaching the water table for uptake. Using the ET package in the numerical model helps eliminate inaccuracies pertaining to ET discharge from vadose zone. Although GW fed ET has decreased, consumptive water use remains high due increased irrigation.
3. The effects of irrigation and land use change cause declines of baseflow and stream discharge at Culbertson by up to 98%. The average stream discharge reduction for the entire simulation time was 39.5%.

4. Calibrated hydraulic conductivity values and stream discharge are in agreement with reported values from the analytical model. However, a significant difference emerged with time between simulated GW inflow values from the two models.
5. The model reproduces trends in streamflow decline according to 3 periods: from 1950 to 1980, the ratio of streamflow decline increased from 18.53% to 48.61% with an average of 32%; from 1981 to 2010 the streamflow decline ratio increased from 53.63% to 65.03% with an average of 56.5%. From 2010 to 2015 there has been a decreasing trend in streamflow decline ratio with average ratio dropping slightly from 65.03% to 58%.

Although the numerical model was able to consistently reproduce baseflow and stream discharge values, some assumptions could potentially be addressed to more accurately depict some of the hydrologic processes. The MODFLOW recharge package applies recharge rates directly to the water table; this assumes that water goes through the vadose zone instantaneously. This assumption is not accurate and can potentially introduces some errors, especially in areas with a deep-water table. (Rossman et al., 2014). The use of MODFLOW Unsaturated Zone Flow (UZF) package (Niswonger et al., 2006) could be useful in solving this problem.

In order to address aquifer heterogeneity, we delineated two different hydraulic conductivity zones. Calibration results did suggest different values for both hydraulic conductivity and storage coefficients. However, accepting only two homogeneous zones may still be an oversimplification. Test hole data and irrigation well logs from Lappala (1978) and Peckenpaugh et al., (1995) suggest a more heterogeneous aquifer than our sedimentological model. The consequences of simplifications can be assessed using the pilot point method in the calibration process.

References

Anderson, M. P. (1982). Introduction to groundwater modeling: finite difference and finite element methods. Freeman.

Anderson, M. P., Woessner, W. W., & Hunt, R. J. (2015). Applied groundwater modeling: simulation of flow and advective transport. Academic press.Barlow, P. M., & Harbaugh, A. W. (2006). USGS directions in MODFLOW development. Groundwater, 44(6), 771-774.

Barlow, Paul M., William L. Cunningham, Tong Zhai, and Mark Gray. US Geological Survey groundwater toolbox, a graphical and mapping interface for analysis of hydrologic data (version 1.0): user guide for estimation of base flow, runoff, and groundwater recharge from streamflow data. No. 3-B10. US Geological Survey, 2015.

Bellot, J., Bonet, A., Sanchez, J. R., & Chirino, E. (2001). Likely effects of land use changes on the runoff and aquifer recharge in a semiarid landscape using a hydrological model. Landscape and Urban Planning, 55(1), 41-53.

Bouwer, H., & Rice, R. C. (1976). A slug test for determining hydraulic conductivity of unconfined aquifers with completely or partially penetrating wells. Water resources research, 12(3), 423-428.

Bosch-Rubia, G. (2015). Land Use and Water and Soil Management Practices Impacts on Potential Groundwater Recharge in Loess Regions of South Central Nebraska.

Burchett, R. R. (1986). Geologic bedrock map of Nebraska: Conservation and Survey Division. *University of Nebraska-Lincoln, scale, 1*(1,000,000).

Burt, O. R., Baker, M., & Helmers, G. A. (2002). Statistical estimation of streamflow depletion from irrigation wells. *Water Resources Research*, *38*(12).

Butler, J. J., & Healey, J. M. (1998). Relationship Between Pumping-Test and Slug-Test Parameters: Scale Effect or Artifact?. *Groundwater*, *36*(2), 305-312.

Cardwell, W. D. E., Jenkins, E. D., Jochens, E. R., & Krieger, R. A. (1963). *Ground-water geology and pump irrigation in Frenchman Creek basin above Palisade, Nebraska*. US Government Printing Office.

Chen, X., & Yin, Y. (2001). STREAMFLOW DEPLETION: MODELING OF REDUCED BASEFLOW ANI INDUCED STREAM INFILTRATION FROM SEASONALLY PUMPED WELLS 1. *JAWRA Journal of the American Water Resources Association*, *37*(1), 185-195.

Condra, G. E. (1907). *Geology and water resources of the Republican River Valley and adjacent areas, Nebraska* (No. 216). USGPO,. Diffendal, R. F. (1991). Geologic map showing configuration of the bedrock surface, North Platte, 1 degree x 2 degrees quadrangle, Nebraska.

Dewandel, B., Gandolfi, J. M., De Condappa, D., & Ahmed, S. (2008). An efficient methodology for estimating irrigation return flow coefficients of irrigated crops at watershed and seasonal scale. Hydrological Processes: An International Journal, 22(11), 1700-1712.

Diersch, H. J. G. (2005). FEFLOW finite element subsurface flow and transport simulation system. *Inst. for Water Resources Planning and System Res., Berlin*.

Diffendal, R. F. (1991). Geologic map showing configuration of the bedrock surface, North Platte, 1 degree x 2 degrees quadrangle, Nebraska.

Dripps, W. R., & Bradbury, K. R. (2007). A simple daily soil–water balance model for estimating the spatial and temporal distribution of groundwater recharge in temperate humid areas. Hydrogeology Journal, 15(3), 433-444.

Dripps, W., Anderson, M. P., & Potter, K. W. (2001). Temporal and spatial variability of natural groundwater recharge. University of Wisconsin Water Resources Institute.

Fenneman, N. M. (1931). *Physiography of Western United Stateds*. Mcgraw-Hill Book Company, Inc.; New York.

Fetter, Charles Willard. Applied hydrogeology. Waveland Press, 2018.

Fredlund, M. D. (2010). User's Manual for SVFlux, Saturated-Unsaturated Numerical Modeling. *SoilVision Systems, Saskatoon, Canada*.

Freeze, R.A. and Cherry, J.A. 1979. Groundwater. Prentice Hall Fox, G. 2004. Evaluation of a stream aquifer analysis test using analytical solutions and field data. Journal of American Water Resources Association 40, no. 3: 755-763

Hendricks, M. (2010). *Introduction to physical hydrology*. Oxford University Press.

Haitjema, T., Disch, F., Overtoom, T. T., Westermann, C. J., & Lammers, J. W. (1995). Screening family members of patients with hereditary hemorrhagic telangiectasia. *The American journal of medicine*, *99*(5), 519-524.

Hanson, R. T., Boyce, S. E., Schmid, W., Hughes, J. D., Mehl, S. W., Leake, S. A., ... & Niswonger, R. G. (2014). *One-water hydrologic flow model (MODFLOW-OWHM)* (No. 6-A51). US Geological Survey.

Harbaugh, A. W. (2005). MODFLOW-2005, the US Geological Survey modular ground-water model: the ground-water flow process (p. 253). Reston, VA: US Department of the Interior, US Geological Survey.

Harbaugh, A. W., Banta, E. R., Hill, M. C., & McDonald, M. G. (2000). MODFLOW-2000, The U. S. Geological Survey Modular Ground-Water Model-User Guide to Modularization Concepts and the Ground-Water Flow Process. *Open-file Report. U. S. Geological Survey*, (92), 134.

Harbaugh, A. W., & McDonald, M. G. (1996). Programmer's documentation for MODFLOW-96, an update to the US Geological Survey modular finite-difference ground-water flow model (No. 96-486). US Geological Survey; Branch of Information Services [distributor],.

Hendriks, M. (2010). *Introduction to physical hydrology*. Oxford University Press.

Kollet, S. J., & Zlotnik, V. A. (2003). Stream depletion predictions using pumping test data from a heterogeneous stream–aquifer system (a case study from the Great Plains, USA). Journal of Hydrology, 281(1-2), 96-114.

Langevin, C. D., Hughes, J. D., Banta, E. R., Niswonger, R. G., Panday, S., & Provost, A. M. (2017). *Documentation for the MODFLOW 6 Groundwater Flow Model* (No. 6-A55). US Geological Survey.

Lappala, E. G. (1978). Quantitative hydrogeology of the Upper Republican natural resources district, southwest Nebraska(No. 78-38). US Geological Survey.

Leopold, L. B. (1968). Hydrology for urban land planning: A guidebook on the hydrologic effects of urban land use.

McDonald, M. G., & Harbaugh, A. W. (1988). *A modular three-dimensional finite-difference ground-water flow model* (Vol. 6, p. A1). Reston, VA: US Geological Survey.

McDonald, M. G., Harbaugh, A. W. (2003) original authors of MODFLOW. The history of MODFLOW. *Groundwater*, *41*(2), 280-283.

McGuire, V.L., (2014), Water-level changes and change in water in storage in the High Plains aquifer, predevelopment to 2013 and 2011–13: U.S. Geological Survey Scientific Investigations Report 2014–5218, 14 p. [Also available at http://dx.doi.org/10.3133/sir20145218.]

Mehl, S. W., & Hill, M. C. (2006). MODFLOW-2005, the US Geological Survey modular ground-water model-documentation of shared node local grid refinement (LGR) and the boundary flow and head (BFH) package (No. 6-A12).

Moore, C., & Doherty, J. (2006). The cost of uniqueness in groundwater model calibration. Advances in Water Resources, 29(4), 605-623.

Niswonger, R. G., Panday, S., & Ibaraki, M. (2011). MODFLOW-NWT, a Newton formulation for MODFLOW-2005. *US Geological Survey Techniques and Methods*, *6*(A37), 44.

Niswonger, R. G., Prudic, D. E., & Regan, R. S. (2006). Documentation of the unsaturated-zone flow (UZF1) package for modeling unsaturated flow between the land surface and the water table with MODFLOW-2005 (No. 6-A19).

Panday, S., Langevin, C. D., Niswonger, R. G., Ibaraki, M., & Hughes, J. D. (2013). MODFLOW–USG version 1: An unstructured grid version of MODFLOW for simulating groundwater flow and tightly coupled processes using a control volume finite-difference formulation (No. 6-A45). US Geological Survey.

Peckenpaugh, J. M., Kern, R. A., Dugan, J. T., & Kilpatrick, J. M. (1995). Simulated response of the High Plains aquifer to ground-water withdrawals in the Upper Republican Natural Resources District, Nebraska. US Department of the Interior, US Geological Survey.

Peterson, S. M., Flynn, A. T., & Traylor, J. P. (2016). Groundwater-Flow Model of the Northern High Plains Aquifer in Colorado, Kansas, Nebraska, South Dakota, and Wyoming (No. 2016-5153). US Geological Survey.

Reimann, T., & Hill, M. E. (2009). MODFLOW-CFP: A New Conduit Flow Process for MODFLOW–2005. *Groundwater*, *47*(3), 321-325.

Republican River Groundwater Modeling Committee. 2003. Republican River Compact Administration Ground Water Model. June 30, 2003. Retrieved on July 12, 2018 from http://www.republicanrivercompact.org/v12p/html/ch02.html

Rossman, N. R., & Zlotnik, V. A. (2013). Regional groundwater flow modeling in heavily irrigated basins of selected states in the western United States. *Hydrogeology Journal*, *21*(6), 1173-1192.

Rossman, N. R., Zlotnik, V. A., Rowe, C. M., & Szilagyi, J. (2014). Vadose zone lag time and potential 21st century climate change effects on spatially distributed groundwater recharge in the semi-arid Nebraska Sand Hills. Journal of Hydrology, 519, 656-669.

Scanlon, B. R., Reedy, R. C., Stonestrom, D. A., Prudic, D. E., & Dennehy, K. F. (2005). Impact of land use and land cover change on groundwater recharge and quality in the southwestern US. Global Change Biology, 11(10), 1577-1593.

Schmid, W., Hanson, R. T., Maddock III, T., & Leake, S. A. (2006). User guide for the farm process (FMP1) for the US Geological Survey's modular three-dimensional finite-difference ground-water flow model, MODFLOW-2000. *US Geological Survey Techniques and Methods*, 6-A17.

Smith, E. A., & Westenbroek, S. M. (2015). Potential groundwater recharge for the State of Minnesota using the Soil-Water-Balance model, 1996-2010 (No. 2015-5038, p. 85). US Geological Survey.

Sohl, T. L., Sayler, K. L., Drummond, M. A., & Loveland, T. R. (2007). The FORE-SCE model: a practical approach for projecting land cover change using scenario-based modeling. *Journal of Land Use Science*, *2*(2), 103-126.

Stanton, J. S., Qi, S. L., Ryter, D. W., Falk, S. E., Houston, N. A., Peterson, S. M., ... & Christenson, S. C. (2011). Selected approaches to estimate water-budget components of the High Plains, 1940 through 1949 and 2000 through 2009. US Geol. Surv. Sci. Invest. Rep, 5183, 79.

Szilagyi, J. (1999). Streamflow depletion investigations in the Republican River basin: Colorado, Nebraska, and Kansas. *Journal of Environmental Systems*, *27*(3), 251-263.

Szilagyi, J. (2001). Identifying cause of declining flows in the Republican River. *Journal of water resources planning and management*, *127*(4), 244-253.

Traylor, J. P., & Zlotnik, V. A. (2016). Analytical modeling of irrigation and land use effects on streamflow in semi-arid conditions. *Journal of Hydrology*, *533*, 591-602.

Traylor, J. P. (2012) Analytical modeling of irrigation and land use effects on streamflow in semi-arid conditions: Frenchman Creek, Nebraska. Master thesis, University of Nebraska Lincoln. Accessed from https://digitalcommons.unl.edu/geoscidiss/32/

U.S. Geological Survey (2018). Ogallala Group or Formation. Retrieved May 19, 2018 from https://mrdata.usgs.gov/geology/state/sgmc-unit.php?unit=NETo%3B0

Wang, H. F., & Anderson, M. P. (1995). Introduction to groundwater modeling: finite difference and finite element methods. Academic Press.

Westenbroek, S. M., Kelson, V. A., Dripps, W. R., Hunt, R. J., & Bradbury, K. R. (2010). SWB--a modified Thornthwaite-Mather soil-water-balance code for estimating groundwater recharge (p. 60). Reston, VA: US Department of the Interior, US Geological Survey, Ground Resources Program.

Zeng, R., & Cai, X. (2014). Analyzing streamflow changes: Irrigation-enhanced interaction between aquifer and streamflow in the Republican River Basin. *Hydrology and Earth System Sciences*, *18*(2), 493-502.

Zlotnik, V. (1994). Interpretation of slug and packer tests in anisotropic aquifers. *Groundwater*, *32*(5), 761-766.

Zyvoloski, A. George (2007). FEHM: A control volume finite element code for simulating subsurface multi-phase multi-fluid heat and mass transfer (Report). Los Alamos Unclassified Report LA-UR-07-3359.

APPENDICES FOR SUPPLEMENTAL MATERIALS

Appendix A: Irrigation, streamflow and ET in ase and disturbed conditions

This composite graph helps visualize and directly compare base condition to disturbed one. With low irrigation in base condition, stream outflow at Culbertson is higher than in disturbed condition. Evapotranspiration response to disturbed condition can be easily assessed as it remains high in base condition whereas in disturbed conditions, it is responsive to groundwater level decline.

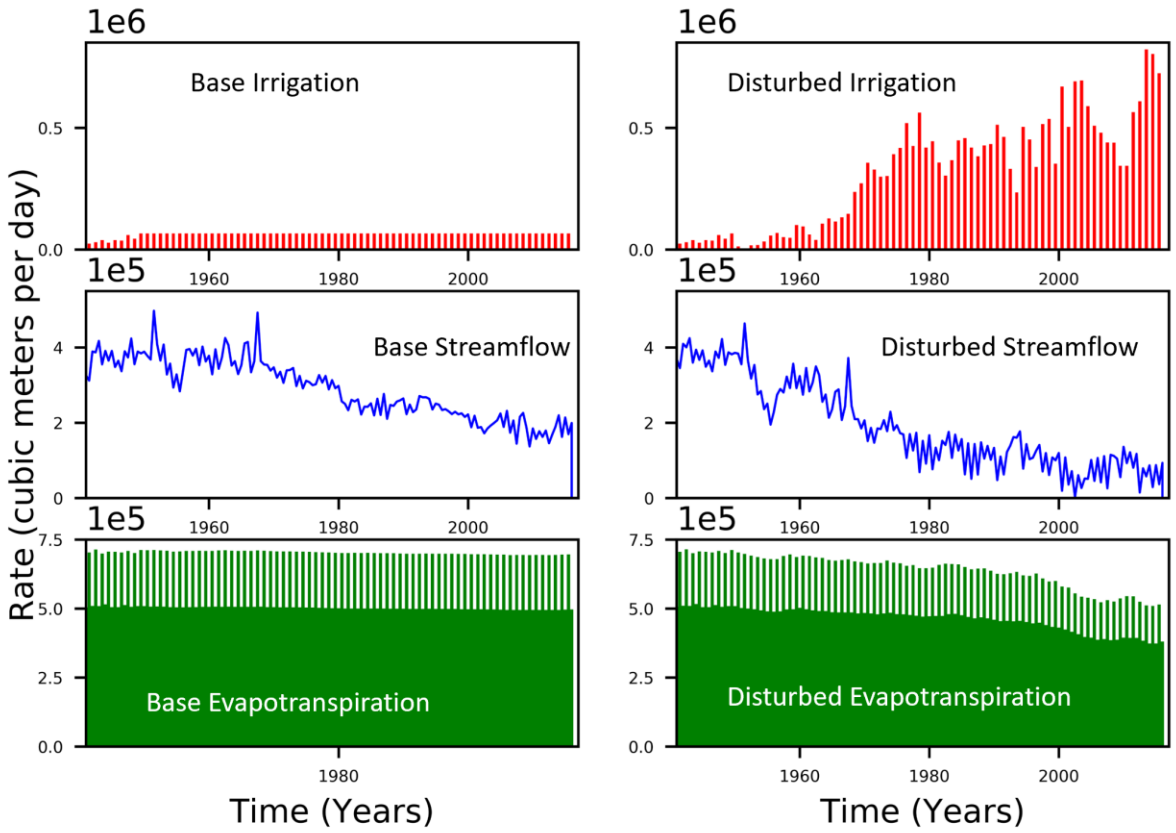

Figure A-1. Irrigation in base and disturbed conditions are on the top; streamflow out of Culbertson in the middle and evapotranspiration at the bottom. Graphs on the left are base condition and the ones on the right are disturbed condition

Appendix B: GW inflow, baseflow and storage changes in base and disturbed conditions

GW inflow to the basin in base condition is high all the time and suggests that transmissivity remains high. This has a direct effect on baseflow as conceptual model suggests that a significant part of GW inflow eventually discharges to stream as baseflow when heavy pumping does not occur. Disturbed condition change in storage shows how land use change and irrigation make the aquifer instable

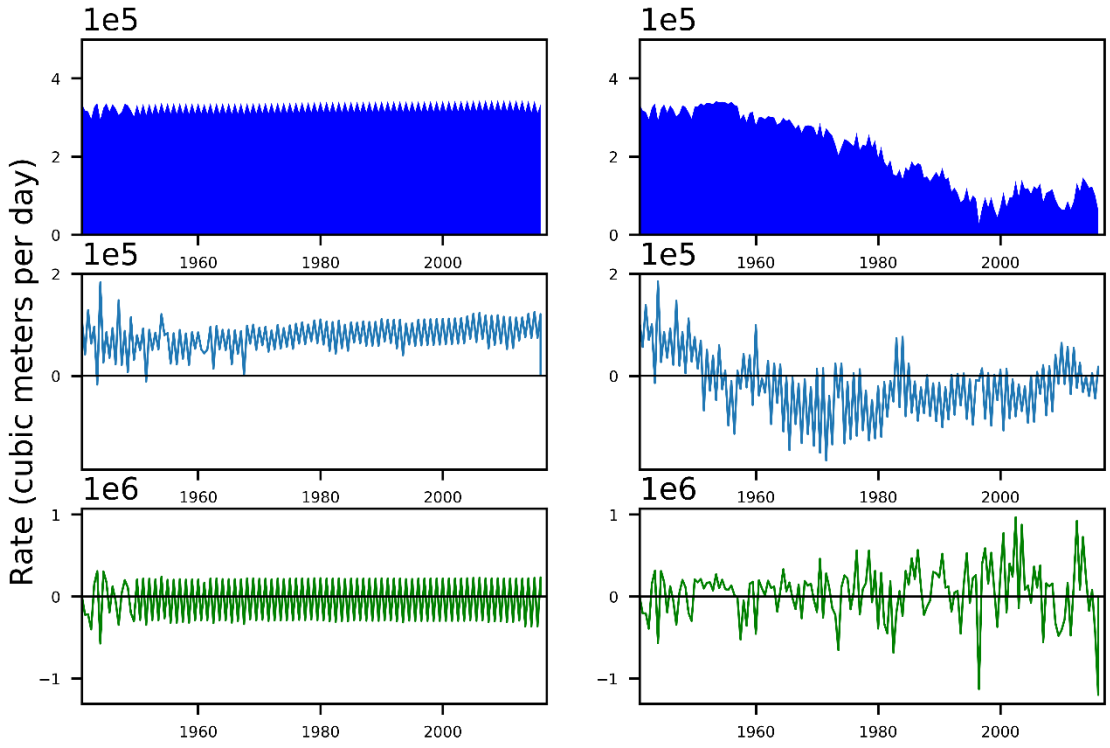

Figure B-1. GW inflows are on the top. Baseflow in the middle and change in storage at the bottom. Base fluxes are on the left and disturbed condition fluxes are on the right.

Appendix C: Stream discharge in base and disturbed conditions

Superposition of simulated stream outflow at Culbertson in base and disturbed conditions allows for immediate assessment of streamflow decline over the simulation period. in bluebase condition and in green in disturbed condition outflow. Simulated values start out identically but outflow in disturbed condition declines faster than base condition outflow

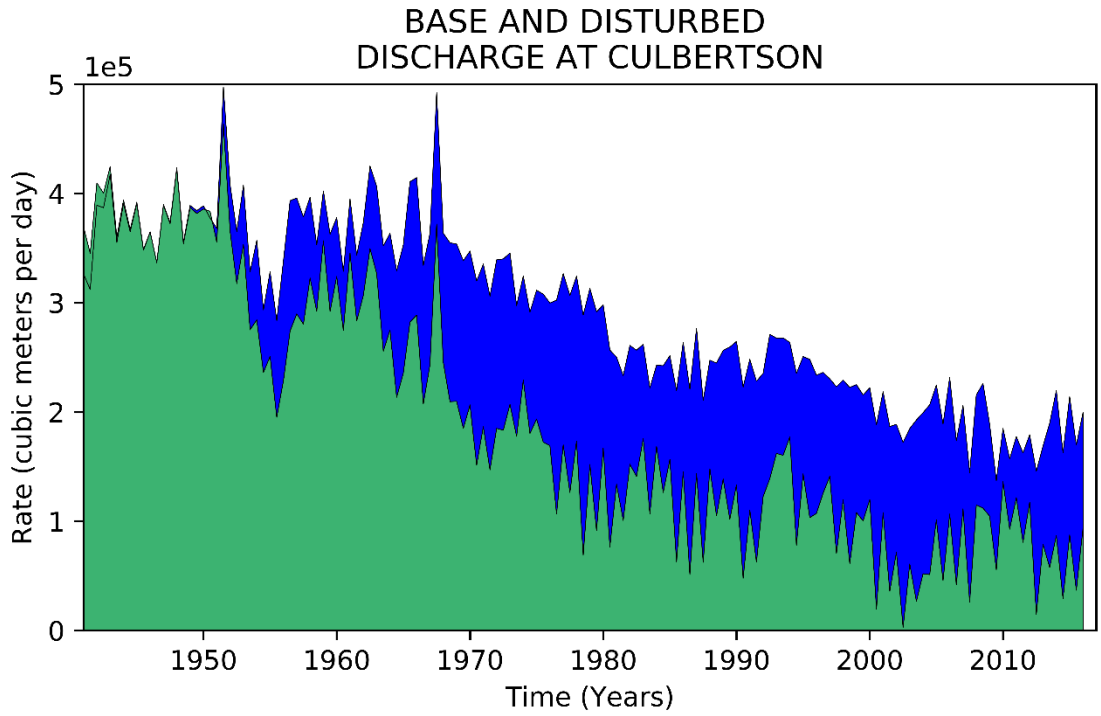

Figure C-1:Base and disturbed streamflow at Culbertson

Appendix D: Start and end date for each stress period.

Stress Period Number	Designation	Start date	End date	Duration [days]	Number of time steps
1	Non-Growing 1941	1/1/1941	4/30/1941	120	10
2	Growing season 1941	5/1/1941	9/30/1941	153	11
3	Non-Growing 1942	10/1/1941	4/30/1942	212	15
4	Growing season 1942	5/1/1942	9/30/1942	153	11
5	Non-Growing 1943	10/1/1942	4/30/1943	212	15
6	Growing season 1943	5/1/1943	9/30/1943	153	11
7	Non-Growing 1944	10/1/1943	4/30/1944	213	15
8	Growing season 1944	5/1/1944	9/30/1944	153	11
9	Non-Growing 1945	10/1/1944	4/30/1945	212	15
10	Growing season 1945	5/1/1945	9/30/1945	153	11
11	Non-Growing 1946	10/1/1945	4/30/1946	212	15
12	Growing season 1946	5/1/1946	9/30/1946	153	11
13	Non-Growing 1947	10/1/1946	4/30/1947	212	15
14	Growing season 1947	5/1/1947	9/30/1947	153	11
15	Non-Growing 1948	10/1/1947	4/30/1948	213	15
16	Growing season 1948	5/1/1948	9/30/1948	153	11
17	Non-Growing 1949	10/1/1948	4/30/1949	212	15
18	Growing season 1949	5/1/1949	9/30/1949	153	11
19	Non-Growing 1950	10/1/1949	4/30/1950	212	15
20	Growing season 1950	5/1/1950	9/30/1950	153	11
21	Non-Growing 1951	10/1/1950	4/30/1951	212	15
22	Growing season 1951	5/1/1951	9/30/1951	153	11
23	Non-Growing 1952	10/1/1951	4/30/1952	213	15
24	Growing season 1952	5/1/1952	9/30/1952	153	11
25	Non-Growing 1953	10/1/1952	4/30/1953	212	15
26	Growing season 1953	5/1/1953	9/30/1953	153	11
27	Non-Growing 1954	10/1/1953	4/30/1954	212	15
28	Growing season 1954	5/1/1954	9/30/1954	153	11
29	Non-Growing 1955	10/1/1954	4/30/1955	212	15
30	Growing season 1955	5/1/1955	9/30/1955	153	11
31	Non-Growing 1956	10/1/1955	4/30/1956	213	15
32	Growing season 1956	5/1/1956	9/30/1956	153	11
33	Non-Growing 1957	10/1/1956	4/30/1957	212	15
34	Growing season 1957	5/1/1957	9/30/1957	153	11
35	Non-Growing 1958	10/1/1957	4/30/1958	212	15
36	Growing season 1958	5/1/1958	9/30/1958	153	11
37	Non-Growing 1959	10/1/1958	4/30/1959	212	15
38	Growing season 1959	5/1/1959	9/30/1959	153	11
39	Non-Growing 1960	10/1/1959	4/30/1960	213	15
40	Growing season 1960	5/1/1960	9/30/1960	153	11
41	Non-Growing 1961	10/1/1960	4/30/1961	212	15
42	Growing season 1961	5/1/1961	9/30/1961	153	11
43	Non-Growing 1962	10/1/1961	4/30/1962	212	15
44	Growing season 1962	5/1/1962	9/30/1962	153	11
45	Non-Growing 1963	10/1/1962	4/30/1963	212	15
46	Growing season 1963	5/1/1963	9/30/1963	153	11
47	Non-Growing 1964	10/1/1963	4/30/1964	213	15
48	Growing season 1964	5/1/1964	9/30/1964	153	11
49	Non-Growing 1965	10/1/1964	4/30/1965	212	15
50	Growing season 1965	5/1/1965	9/30/1965	153	11

Stress Period Number	Designation	Start date	End date	Duration [days]	Number of time steps
51	Non-Growing 1966	10/1/1965	4/30/1966	212	15
52	Growing season 1966	5/1/1966	9/30/1966	153	11
53	Non-Growing 1967	10/1/1966	4/30/1967	212	15
54	Growing season 1967	5/1/1967	9/30/1967	153	11
55	Non-Growing 1968	10/1/1967	4/30/1968	213	15
56	Growing season 1968	5/1/1968	9/30/1968	153	11
57	Non-Growing 1969	10/1/1968	4/30/1969	212	15
58	Growing season 1969	5/1/1969	9/30/1969	153	11
59	Non-Growing 1970	10/1/1969	4/30/1970	212	15
60	Growing season 1970	5/1/1970	9/30/1970	153	11
61	Non-Growing 1971	10/1/1970	4/30/1971	212	15
62	Growing season 1971	5/1/1971	9/30/1971	153	11
63	Non-Growing 1972	10/1/1971	4/30/1972	213	15
64	Growing season 1972	5/1/1972	9/30/1972	153	11
65	Non-Growing 1973	10/1/1972	4/30/1973	212	15
66	Growing season 1973	5/1/1973	9/30/1973	153	11
67	Non-Growing 1974	10/1/1973	4/30/1974	212	15
68	Growing season 1974	5/1/1974	9/30/1974	153	11
69	Non-Growing 1975	10/1/1974	4/30/1975	212	15
70	Growing season 1975	5/1/1975	9/30/1975	153	11
71	Non-Growing 1976	10/1/1975	4/30/1976	213	15
72	Growing season 1976	5/1/1976	9/30/1976	153	11
73	Non-Growing 1977	10/1/1976	4/30/1977	212	15
74	Growing season 1977	5/1/1977	9/30/1977	153	11
75	Non-Growing 1978	10/1/1977	4/30/1978	212	15
76	Growing season 1978	5/1/1978	9/30/1978	153	11
77	Non-Growing 1979	10/1/1978	4/30/1979	212	15
78	Growing season 1979	5/1/1979	9/30/1979	153	11
79	Non-Growing 1980	10/1/1979	4/30/1980	213	15
80	Growing season 1980	5/1/1980	9/30/1980	153	11
81	Non-Growing 1981	10/1/1980	4/30/1981	212	15
82	Growing season 1981	5/1/1981	9/30/1981	153	11
83	Non-Growing 1982	10/1/1981	4/30/1982	212	15
84	Growing season 1982	5/1/1982	9/30/1982	153	11
85	Non-Growing 1983	10/1/1982	4/30/1983	212	15
86	Growing season 1983	5/1/1983	9/30/1983	153	11
87	Non-Growing 1984	10/1/1983	4/30/1984	213	15
88	Growing season 1984	5/1/1984	9/30/1984	153	11
89	Non-Growing 1985	10/1/1984	4/30/1985	212	15
90	Growing season 1985	5/1/1985	9/30/1985	153	11
91	Non-Growing 1986	10/1/1985	4/30/1986	212	15
92	Growing season 1986	5/1/1986	9/30/1986	153	11
93	Non-Growing 1987	10/1/1986	4/30/1987	212	15
94	Growing season 1987	5/1/1987	9/30/1987	153	11
95	Non-Growing 1988	10/1/1987	4/30/1988	213	15
96	Growing season 1988	5/1/1988	9/30/1988	153	11
97	Non-Growing 1989	10/1/1988	4/30/1989	212	15
98	Growing season 1989	5/1/1989	9/30/1989	153	11
99	Non-Growing 1990	10/1/1989	4/30/1990	212	15
100	Growing season 1990	5/1/1990	9/30/1990	153	11

Stress Period Number	Designation	Start date	End date	Duration [days]	Number of time steps
101	Non-Growing 1991	10/1/1990	4/30/1991	212	15
102	Growing season 1991	5/1/1991	9/30/1991	153	11
103	Non-Growing 1992	10/1/1991	4/30/1992	213	15
104	Growing season 1992	5/1/1992	9/30/1992	153	11
105	Non-Growing 1993	10/1/1992	4/30/1993	212	15
106	Growing season 1993	5/1/1993	9/30/1993	153	11
107	Non-Growing 1994	10/1/1993	4/30/1994	212	15
108	Growing season 1994	5/1/1994	9/30/1994	153	11
109	Non-Growing 1995	10/1/1994	4/30/1995	212	15
110	Growing season 1995	5/1/1995	9/30/1995	153	11
111	Non-Growing 1996	10/1/1995	4/30/1996	213	15
112	Growing season 1996	5/1/1996	9/30/1996	153	11
113	Non-Growing 1997	10/1/1996	4/30/1997	212	15
114	Growing season 1997	5/1/1997	9/30/1997	153	11
115	Non-Growing 1998	10/1/1997	4/30/1998	212	15
116	Growing season 1998	5/1/1998	9/30/1998	153	11
117	Non-Growing 1999	10/1/1998	4/30/1999	212	15
118	Growing season 1999	5/1/1999	9/30/1999	153	11
119	Non-Growing 2000	10/1/1999	4/30/2000	213	15
120	Growing season 2000	5/1/2000	9/30/2000	153	11
121	Non-Growing 2001	10/1/2000	4/30/2001	212	15
122	Growing season 2001	5/1/2001	9/30/2001	153	11
123	Non-Growing 2002	10/1/2001	4/30/2002	212	15
124	Growing season 2002	5/1/2002	9/30/2002	153	11
125	Non-Growing 2003	10/1/2002	4/30/2003	212	15
126	Growing season 2003	5/1/2003	9/30/2003	153	11
127	Non-Growing 2004	10/1/2003	4/30/2004	213	15
128	Growing season 2004	5/1/2004	9/30/2004	153	11
129	Non-Growing 2005	10/1/2004	4/30/2005	212	15
130	Growing season 2005	5/1/2005	9/30/2005	153	11
131	Non-Growing 2006	10/1/2005	4/30/2006	212	15
132	Growing season 2006	5/1/2006	9/30/2006	153	11
133	Non-Growing 2007	10/1/2006	4/30/2007	212	15
134	Growing season 2007	5/1/2007	9/30/2007	153	11
135	Non-Growing 2008	10/1/2007	4/30/2008	213	15
136	Growing season 2008	5/1/2008	9/30/2008	153	11
137	Non-Growing 2009	10/1/2008	4/30/2009	212	15
138	Growing season 2009	5/1/2009	9/30/2009	153	11
139	Non-Growing 2010	10/1/2009	4/30/2010	212	15
140	Growing season 2010	5/1/2010	9/30/2010	153	11
141	Non-Growing 2011	10/1/2010	4/30/2011	212	15
142	Growing season 2011	5/1/2011	9/30/2011	153	11
143	Non-Growing 2012	10/1/2011	4/30/2012	213	15
144	Growing season 2012	5/1/2012	9/30/2012	153	11
145	Non-Growing 2013	10/1/2012	4/30/2013	212	15
146	Growing season 2013	5/1/2013	9/30/2013	153	11
147	Non-Growing 2014	10/1/2013	4/30/2014	212	15
148	Growing season 2014	5/1/2014	9/30/2014	153	11
149	Non-Growing 2015	10/1/2014	4/30/2015	212	15
150	Growing season 2015	5/1/2015	9/30/2015	153	11
151	Non-Growing 2016	10/1/2015	12/31/2015	92	10

Appendix E: Instructions for model reconstruction

This section shows steps in reconstruction and run the MODFLOW in parameter estimation model. MODFLOW and PEST use pre-processed input files to solve for the unknown. All required files are provided in appendix F as a zip file and attached to this document (FC_MODFLOW6.zip). It is crucial that each file be placed in the designated folder (see model tree below) in order for the model to run. If all instructions are followed correctly, the model should run without an issue and the outputs could be used to reproduce the graphs in this document. Below are the steps:

1. Download FC_MODFLOW6.zip
2. Extract content to FC_MODFLOW6 and create the following subfolders; all words and names are case sensitive.
    a. bin: be sure to keep lower case “b”
    b. FRENCHMAN_CREEK
        i. model (lowercase “m”)
            1. ancill
            2. irrig
            3. CDH
            4. sfr
        ii. output
            1. cal
            2. ZBud-direct
        iii. Pest
            1. instpl

iv. Zonebudget

3. Place each file in the appropriate folder. The tables below grouped files by destination folder
4. To run the model in parameter estimation mode, go to the pest directory, find the batch file named runPest.bat and double click on it. It take approximately 8 hours for optimization.
5. To run the model only, go to folder named “model”, find the batch file runFrenchmanCreeck.bat and double click on it. It take approximately 7 minutes for the model to run to completion.
6. We have included some batch files and python files in the chain of run to automate some post processing tasks. Thus, after every model is run, zone budget runs and saves a csv files in this directory: FC_MODFLOW6\FRENCHMAN_CREECK\output\ZBud-direct as fcbud.csv
7. The csv file contains all inflows and outflows for each budget component.

The following tables group the files by destination folder.

bin
i64pest.exe
mf6.exe
pest.exe
zbud6.exe

sfr
sfr_packagedata.dat

model
disv.bot_layer4.dat
disv.cell2d.dat
disv.top.dat
disv.top_layer.dat
disv.verts.dat
fc.chd
fc.disv
fc.disv.grb
fc.evt
fc.heads_obs.out
fc.ic
fc.ims
fc.lst
fc.mv
fc.nam
fc.npf
fc.obs
fc.oc
fc.rch
fc.sfr
fc.sto
fc.tdis
fc.wel
fc_sfr.obs
fc_sfr_Mar.obs
fc_SS.dat
fc_SY.dat
Kxy.fc.dat
Kzz.fc.dat
MFcalledbyPest.bat
mfsim.lst
mfsim.nam
oclisting.txt
runFrenchmanCreek.bat
sfr.enders.obs.txt

ancill
R_1_1941.txt
R_1_1942.txt
R_1_1943.txt
R_1_1944.txt
R_1_1945.txt
R_1_1946.txt
R_1_1947.txt
R_1_1948.txt
R_1_1949.txt
R_1_1950.txt
R_1_1951.txt
R_1_1952.txt
R_1_1953.txt
R_1_1954.txt
R_1_1955.txt
R_1_1956.txt
R_1_1957.txt
R_1_1958.txt
R_1_1959.txt
R_1_1960.txt
R_1_1961.txt
R_1_1962.txt
R_1_1963.txt
R_1_1964.txt
R_1_1965.txt
R_1_1966.txt
R_1_1967.txt
R_1_1968.txt
R_1_1969.txt
R_1_1970.txt
R_1_1971.txt
R_1_1972.txt
R_1_1973.txt
R_1_1974.txt
R_1_1975.txt

R_1_1976.txt
R_1_1977.txt
R_1_1978.txt
R_1_1979.txt
R_1_1980.txt
R_1_1981.txt
R_1_1982.txt
R_1_1983.txt
R_1_1984.txt
R_1_1985.txt
R_1_1986.txt
R_1_1987.txt
R_1_1988.txt
R_1_1989.txt
R_1_1990.txt
R_1_1991.txt
R_1_1992.txt
R_1_1993.txt
R_1_1994.txt
R_1_1995.txt
R_1_1996.txt
R_1_1997.txt
R_1_1998.txt
R_1_1999.txt
R_1_2000.txt
R_1_2001.txt
R_1_2002.txt
R_1_2003.txt
R_1_2004.txt
R_1_2005.txt
R_1_2006.txt
R_1_2007.txt
R_1_2008.txt
R_1_2009.txt
R_2_1940.txt

R_2_1941.txt
R_2_1942.txt
R_2_1943.txt
R_2_1944.txt
R_2_1945.txt
R_2_1946.txt
R_2_1947.txt
R_2_1948.txt
R_2_1949.txt
R_2_1950.txt
R_2_1951.txt
R_2_1952.txt
R_2_1953.txt
R_2_1954.txt
R_2_1955.txt
R_2_1956.txt
R_2_1957.txt
R_2_1958.txt
R_2_1959.txt
R_2_1960.txt
R_2_1961.txt
R_2_1962.txt
R_2_1963.txt
R_2_1964.txt
R_2_1965.txt
R_2_1966.txt
R_2_1967.txt
R_2_1968.txt
R_2_1969.txt
R_2_1970.txt
R_2_1971.txt
R_2_1972.txt
R_2_1973.txt
R_2_1974.txt
R_2_1975.txt

R_2_1976.txt
R_2_1977.txt
R_2_1978.txt
R_2_1979.txt
R_2_1980.txt
R_2_1981.txt
R_2_1982.txt
R_2_1983.txt
R_2_1984.txt
R_2_1985.txt
R_2_1986.txt
R_2_1987.txt
R_2_1988.txt
R_2_1989.txt
R_2_1990.txt
R_2_1991.txt
R_2_1992.txt
R_2_1993.txt
R_2_1994.txt
R_2_1995.txt
R_2_1996.txt
R_2_1997.txt
R_2_1998.txt
R_2_1999.txt
R_2_2000.txt
R_2_2001.txt
R_2_2002.txt
R_2_2003.txt
R_2_2004.txt
R_2_2005.txt
R_2_2006.txt
R_2_2007.txt
R_2_2008.txt
R_2_2009.txt

CHD
CHD_1941.txt
CHD_1942.txt
CHD_1943.txt
CHD_1944.txt
CHD_1945.txt
CHD_1946.txt
CHD_1947.txt
CHD_1948.txt
CHD_1949.txt
CHD_1950.txt
CHD_1951.txt
CHD_1952.txt
CHD_1953.txt
CHD_1954.txt
CHD_1955.txt
CHD_1956.txt
CHD_1957.txt
CHD_1958.txt
CHD_1959.txt
CHD_1960.txt
CHD_1961.txt
CHD_1962.txt
CHD_1963.txt
CHD_1964.txt
CHD_1965.txt
CHD_1966.txt
CHD_1967.txt
CHD_1968.txt
CHD_1969.txt
CHD_1970.txt
CHD_1971.txt

CHD_1972.txt
CHD_1973.txt
CHD_1974.txt
CHD_1975.txt
CHD_1976.txt
CHD_1977.txt
CHD_1978.txt
CHD_1979.txt
CHD_1980.txt
CHD_1981.txt
CHD_1982.txt
CHD_1983.txt
CHD_1984.txt
CHD_1985.txt
CHD_1986.txt
CHD_1987.txt
CHD_1988.txt
CHD_1989.txt
CHD_1990.txt
CHD_1991.txt
CHD_1992.txt
CHD_1993.txt
CHD_1994.txt
CHD_1995.txt
CHD_1996.txt
CHD_1997.txt
CHD_1998.txt
CHD_1999.txt
CHD_2000.txt

irrig
irrig.period1.dat
irrperiod10.txt
irrperiod100.txt
irrperiod102.txt
irrperiod104.txt
irrperiod106.txt
irrperiod108.txt
irrperiod110.txt
irrperiod112.txt
irrperiod114.txt
irrperiod116.txt
irrperiod118.txt
irrperiod12.txt
irrperiod120.txt
irrperiod122.txt
irrperiod124.txt
irrperiod126.txt
irrperiod128.txt
irrperiod130.txt
irrperiod132.txt
irrperiod134.txt
irrperiod136.txt
irrperiod138.txt
irrperiod14.txt
irrperiod140.txt
irrperiod142.txt
irrperiod144.txt
irrperiod146.txt
irrperiod148.txt
irrperiod150.1.txt
irrperiod150.txt
irrperiod16.txt
irrperiod18.txt
irrperiod2.txt
irrperiod20.txt
irrperiod22.txt
irrperiod24.txt
irrperiod26.txt
irrperiod28.txt
irrperiod30.txt

irrperiod32.txt
irrperiod34.txt
irrperiod36.txt
irrperiod38.txt
irrperiod4.txt
irrperiod40.txt
irrperiod42.txt
irrperiod44.txt
irrperiod46.txt
irrperiod48.txt
irrperiod50.txt
irrperiod52.txt
irrperiod54.txt
irrperiod56.txt
irrperiod58.txt
irrperiod6.txt
irrperiod60.txt
irrperiod62.txt
irrperiod64.txt
irrperiod66.txt
irrperiod68.txt
irrperiod70.txt
irrperiod72.txt
irrperiod74.txt
irrperiod76.txt
irrperiod78.txt
irrperiod8.txt
irrperiod80.txt
irrperiod82.txt
irrperiod84.txt
irrperiod86.txt
irrperiod88.txt
irrperiod90.txt
irrperiod92.txt
irrperiod94.txt
irrperiod96.txt
irrperiod98.txt
non_irrig.period1.dat
non_irrperiod.txt

output
data_by_SP.py
fc.bud
fc.disv.grb
fc.hed
fc.lst
fc.sfr-evap.out
fc.sfr-stage.out
fc.sfr.out
fcsfr.bud
fcstage.bud
img1.jpg
plot.py
PlotDischarge.m
rundatabySP.bat
timelookup.tx

ZBud-direct
drybaseflws.dat
dryseasontimes.txt
Extractbaseflows.py
fcbud.csv
fcbud.lst
fcbud.nam
fczbud.zon
run-zbnow.bat
runExtractbaseflows.bat
runZonebudDirect.bat
timelookup.txt

cal
fc.heads_obs.out

fc.pst
FrenchmanCreek.bat
instpl
runPest.bat
settings.fig

instpl				
baseflows.ins		wl14152.wls.ins		wl18096.wls.ins
fc.sfr.tpl		wl14178.wls.ins		wl18180.wls.ins
fc_SS.dat.tpl		wl14398.wls.ins		wl18318.wls.ins
fc_SY.dat.tpl		wl14408.wls.ins		wl18484.wls.ins
Kxy.fc.dat.tpl		wl14830.wls.ins		wl18536.wls.ins
Outflowgage.sg.ins		wl15002.wls.ins		wl18583.wls.ins
sfr_packagedata.dat.tpl		wl15009.wls.ins		wl18719.wls.ins
wl10128.wls.ins		wl15165.wls.ins		wl18746.wls.ins
wl10231.wls.ins		wl15259.wls.ins		wl18756.wls.ins
wl10969.wls.ins		wl15325.wls.ins		wl18814.wls.ins
wl11562.wls.ins		wl15366.wls.ins		wl18969.wls.ins
wl11734.wls.ins		wl16182.wls.ins		wl18989.wls.ins
wl11917.wls.ins		wl16747.wls.ins		wl18991.wls.ins
wl11923.wls.ins		wl16748.wls.ins		wl19002.wls.ins
wl12160.wls.ins		wl16787.wls.ins		wl19038.wls.ins
wl1221.wls.ins		wl16921.wls.ins		wl19095.wls.ins
wl12452.wls.ins		wl17042.wls.ins		wl19143.wls.ins
wl12690.wls.ins		wl1712.wls.ins		wl19154.wls.ins
wl13119.wls.ins		wl17159.wls.ins		wl19189.wls.ins
wl13164.wls.ins		wl17197.wls.ins		wl1922.wls.ins
wl13235.wls.ins		wl17200.wls.ins		wl19235.wls.ins
wl13350.wls.ins		wl17201.wls.ins		wl19262.wls.ins
wl13527.wls.ins		wl17364.wls.ins		wl19283.wls.ins
wl13670.wls.ins		wl17399.wls.ins		wl19285.wls.ins
wl13715.wls.ins		wl17576.wls.ins		wl193.wls.ins
wl13838.wls.ins		wl17631.wls.ins		wl19363.wls.ins
wl13856.wls.ins		wl17649.wls.ins		wl19373.wls.ins
wl14027.wls.ins		wl17664.wls.ins		wl19383.wls.ins
wl14113.wls.ins		wl17915.wls.ins		wl19497.wls.ins
wl14116.wls.ins		wl17923.wls.ins		wl19556.wls.ins

instpl				
wl19573.wls.ins		wl3971.wls.ins		wl5531.wls.ins
wl19605.wls.ins		wl4002.wls.ins		wl5552.wls.ins
wl19621.wls.ins		wl4293.wls.ins		wl5553.wls.ins
wl19666.wls.ins		wl4304.wls.ins		wl5665.wls.ins
wl19673.wls.ins		wl4355.wls.ins		wl5696.wls.ins
wl19675.wls.ins		wl4359.wls.ins		wl5707.wls.ins
wl19684.wls.ins		wl4382.wls.ins		wl5873.wls.ins
wl2082.wls.ins		wl4451.wls.ins		wl6053.wls.ins
wl2089.wls.ins		wl4491.wls.ins		wl6071.wls.ins
wl2148.wls.ins		wl4503.wls.ins		wl698.wls.ins
wl2261.wls.ins		wl4524.wls.ins		wl7819.wls.ins
wl2450.wls.ins		wl4535.wls.ins		wl8508.wls.ins
wl2489.wls.ins		wl4601.wls.ins		wl870.wls.ins
wl2515.wls.ins		wl4612.wls.ins		wl8709.wls.ins
wl2540.wls.ins		wl4630.wls.ins		wl880.wls.ins
wl2549.wls.ins		wl4674.wls.ins		wl9145.wls.ins
wl2724.wls.ins		wl4724.wls.ins		wl916.wls.ins
wl2830.wls.ins		wl4730.wls.ins		wl9774.wls.ins
wl2907.wls.ins		wl4849.wls.ins		wl9903.wls.ins
wl2937.wls.ins		wl49.wls.ins		
wl2948.wls.ins		wl4917.wls.ins		
wl3178.wls.ins		wl5027.wls.ins		
wl3179.wls.ins		wl5038.wls.ins		
wl3281.wls.ins		wl5071.wls.ins		
wl3418.wls.ins		wl5085.wls.ins		
wl3457.wls.ins		wl5093.wls.ins		
wl3644.wls.ins		wl5222.wls.ins		
wl3800.wls.ins		wl5264.wls.ins		
wl3816.wls.ins		wl5283.wls.ins		
wl3941.wls.ins		wl5454.wls.ins		